sev and pcu Topological Nets in New Mixed-ligands Imidazole-containing Cu(II) Coordination Frameworks: Crystal Structure, Intermolecular Interactions, Theoretical Calculations, Magnetic Behavior and Biological Activity

Amani Direm[a*], Mohammed S. M. Abdelbaky[b], Koray Sayın[c], Olufunso Abosede[d], Andrea Cornia[e], Santiago García-Granda[b].

[a] Laboratoire des Structures, Propriétés et Interactions Interatomiques LASPI²A, Département des Sciences de la Matière, Faculté des Sciences et de la Technologie, Université ''Abbes Laghrour'', Khenchela 40.000, Algeria.

[b] Departamento de Química Física y Analítica, Universidad de Oviedo – CINN, 33006 Oviedo, Spain.

[c] Department of Chemistry, Faculty of Science, Cumhuriyet University 58140 Sivas, Turkey.

[d] Department of Chemistry, Federal University Otuoke, P.M.B 126, Yenagoa, Bayelsa State, Nigeria.

[e] Department of Chemistry & INSTM Research Unit, University of Modena and Reggio Emilia, Via G. Campi 183, 41125 Modena, Italy

* Corresponding Author   : Amani Direm

E-mail   : amani_direm@yahoo.fr

Tel.   : +213.772.33.02.87

Abstract

Novel mixed-ligands coordination frameworks, namely [Cu(Imd)$_3$(H$_2$Cit)] (**1**) and [Cu(Imd)$_2$(HCit)]·(HImd) (**2**) (with Imd = imidazole, H$_2$Cit = dihydrogencitrate, HCit = hydrogencitrate and HImd = imidazolium) were obtained as a result of the reaction between imidazole, citric acid and copper chloride. The complexes were structurally characterized by elemental analysis, FTIR spectroscopy and X-ray diffraction. The two structures were found to be connected through 3D hydrogen-bonding networks examined by means of the *Hirshfeld* surface analysis which highlighted the presence of O−H···O, N−H···O and C−H···O H-bonds together with the π···lp interactions. A topological analysis of the underlying nets corresponding to the two hydrogen-bonded frameworks was carried out. Moreover, quantum chemical calculations were performed using the HF method with 6-31G(d) and LANL2DZ levels in the gas phase, and therefore the optimized structures, the IR, ^{1}H NMR, ^{13}C NMR spectra, the MEP maps and the electronic structure descriptors were examined in detail. Furthermore, the magnetic properties of (**1**) and (**2**) were also investigated. The complexes showed remarkable antimicrobial and antifungal inhibition activities.

Keywords :

1. Introduction :

The nitrogen atom of the imidazole bears interesting physical and chemical properties that result in different pharmacological activities of the molecule and its derivatives [1]. Therefore, literature revealed that imidazole and its derivatives have been reported to have, analgesic, anti-inflammatory, cardiovascular, anti-neoplastic, antifungal, enzyme inhibition, antiviral and antiulcer activities [2]. Moreover, the parasitic and antiviral activities of aniline derivatives of imidazole have been described in the literature [3].

Imidazole occurs in most of proteins as part of the side chain of histidine and constitutes the binding sites of various transition metal ions in a large number of metalloproteins [4]. Consequently, the bonding between imidazole and transition metal ions is widely known [5] and particularly of considerable interest especially in biological systems [6,7]. In order to understand the special magnetic, spectroscopic properties and the catalytic mechanisms of copper proteins, the study and modeling of the active site of copper-containing proteins has been a field of great interest within the scientific community [10]. Therefore, copper(II)–imidazole systems with different ratios of imidazole to copper have been prepared and investigated by several researchers [9]. Furthermore, being studied as models for copper proteins that contain both functionalities in the side chain [10], some mononuclear copper(II)–imidazole complexes with carboxylate ligands have, in addition, been found to have a variety of pharmacological effects, being as antitumor agents [11] and showing superoxide dismutase and catecholase activities [12]. Thus, the recognition of the strong antitumor activity of the trans bis(acetato) bis(imidazole) copper(II) complex [13] caused the growing interest in the synthesis and characterization of those systems [14].

Despite the huge number of papers dedicated to investigate imidazole complexes involving different carboxylates and different metallic centers (copper [15], cobalt [16], nickel [16d,17], manganese [17d,18], cadmium [19] and ruthenium [20]), however the crystallographic information about imidazole-based complexes containing citrate ligands is rather quite poor; only two hexacoordinated complexes have been reported until now, namely (hexakis(imidazole)-cobalt(II) Δ, Λ bis(tris(imidazole)-(citrato)-cobalt(II)) tetrahydrate $[Co(Im)_6][Co_\Delta(Im)_3(Hcit)][Co_\Lambda(Im)_3(Hcit)] \cdot 4H_2O$ and hexakis(imidazole)-nickel(II) Δ, Λ bis(tris(imidazole)-(citrato)-nickel(II)) tetrahydrate $[Ni(Im)_6][Ni_\Delta(Im)_3(Hcit)]$ $[Ni_\Lambda(Im)_3(Hcit)] \cdot 4H_2O$ (Im = imidazole, H_4cit = citric acid) [21]). As a contribution to this study, we present herein an investigation of two new penta-coordinated copper(II) complexes with mixed-ligands; imidazole and citric acid.

2. Experimental :

2.1. Synthesis

Equimolar quantities of imidazole, citric acid and $CuCl_2$ were mixed together with 20 mL of ethanol in a one-pot reaction. The mixture was stirred at 60 °C for one hour and the resulting blue-coloured solution was filtered out and left at room temperature for several days, leading to light-blue prisms of complex (**1**): $[Cu(Imd)_3(H_2Cit)]$ and blue prismatic crystals of complex (**2**): $[Cu(Imd)_2(HCit)]·(HImd)$. Elemental analysis (C, H and N) for (**1**) calc. (exp.): Cu 13.85, O 24.41, N 18.31 (18.48), C 39.26 (39.31), H 4.17 (4.32) %. Elemental analysis (C, H and N) for (**2**) calc. (exp.): Cu 13.85, O 24.41, N 18.31 (18.57), C 39.26 (39.35), H 4.17 (4.48) %.

2.2. Physical measurements

FTIR spectroscopy

The Fourier transform infrared spectra were recorded on a Perkin-Elmer FTIR spectrophotometer in the range of 4000–400 cm^{-1} by using KBr pellets at room temperature.

Elemental analyses

Elemental analyses (C, H and N) were performed using a Carlo Erba EA1110 CHNS-O automatic analyzer.

Magnetic measurements

The magnetic susceptibility measurements were performed using a Quantum Design PPMS magnetometer while heating from 2 to 300 K at 1 kOe after cooling in absence of the applied field (zero field cooling, ZFC). Both compounds have been compacted and enclosed in polypropylene holder that snaps into the brass through sample holder of the VSM option. No changes have been observed in the samples after performing the magnetic measurements.

2.3. X-ray single-crystal structure analysis

Single-crystal diffraction data were collected at room temperature on a Bruker–Nonius X8 APEX diffractometer with graphite-monochromated Mo Kα radiation (λ = 0.71073 Å). The data collection and the cell refinement were performed with the software APEX2 [22]. Whereas, the data integration and reduction were processed with SAINT software [22]. Calculations were carried out using the *WinGX* software package [23]. All the structures were solved by direct methods using *SIR2014* [24] and refined by full-matrix least-squares calculations against F^2 using *SHELXL2014* [25]. All non-hydrogen atoms were refined

anisotropically. Whereas, all hydrogen atoms were placed in calculated positions and refined using a riding model, with distances constraints of N–H = 0.86 Å and C–H = 0.93, 0.97 Å [U_{iso}(H) = 1.2 U_{eq}(N,C)]. Experimental conditions and X-ray structure information for both synthesized compounds are listed in Table 1. Crystal structures were visualized using *ORTEP-3* [23] and *MERCURY* [26]. Software used to prepare material for publication: *WinGX* [23] and *publCIF* [27].

Table 1.

Crystal data and structure refinement parameters for complexes (**1**) and (**2**).

Crystal Data	Complex (**1**)	Complex (**2**)
Chemical formula	$C_{15}H_{18}N_6O_7Cu$	$C_{15}H_{18}N_6O_7Cu$
Formula weight (g·mol^{-1})	457.89	457.89
Crystal system	Monoclinic	Triclinic
Space group	$P2_1/n$	P-1
Temperature (K)	293	293
Unit cell dimensions (Å,°) a b c α β γ	9.0360(2), 23.6063(5), 9.0842(2), - 110.257(1) -	9.2169 (4), 9.3738 (4), 11.8153 (5), 87.704 (1), 83.425 (1), 64.936 (1)
Volume (Å^3)	1817.87(7)	918.56 (7)
Z	4	2
Radiation type	Mo $K\alpha$	Mo $K\alpha$
Calculated density (g·cm^{-3})	1.673	1.656
Absorption coefficient (mm^{-1})	1.26	1.24
Crystal size (mm^3)	0.20 × 0.25 × 0.25	0.20 × 0.20 × 0.25
Color	Light-Blue	Blue
Shape	Prism	Prism
Data collection		
Diffractometer	Bruker–Nonius X8APEX	Bruker–Nonius X8APEX
θ_{max}-θ_{min} (°)	32.0–1.7	32.0–1.7

Measured reflections	29009	11437
Independent reflections	6331	6357
Reflections with I > 2σ(I)	5272	5369
R_{int}	0.029	0.018
h k l	−13→12 −35→33 −13→13	−13→10 −13→13 −17→16
Refinement		
$R[F^2 > 2\sigma(F^2)]$	0.030	0.033
$wR(F^2)$	0.124	0.128
Goodness of feet	1.17	1.18
No. of reflections	6296	6202
No. of parameters	262	262
H-atom treatment	H-atom parameters constrained	H-atom parameters constrained
$\Delta\rho_{max}$, $\Delta\rho_{min}$ (e Å^{-3})	0.68, −1.11	0.79, −0.82

2.4. DFT calculations

Computational calculations were performed by GaussView 5.0.9 [28] and Gaussian 09 AS64L-G09RevD.01 [29] programs. *Hartree-Fock* (HF) method was thus adopted with a mix basis set. At this stage, LANL2DZ was used for metal atoms and 6-31G(d) was used for the remaining atoms. The NMR spectra of the compounds were calculated with gauge-independent atomic orbital (GIAO) method. In calculation stage of chemical shift values, tetramethylsilane (TMS) was used as a reference substance. In calculations of MEP maps, electrostatic potential (ESP) charges were taken into consideration. Additionally, related electronic structure descriptors were calculated by using equations (1) – (5).

$$I = -E_{SOMO} \tag{1}$$

$$A = -E_{LUMO} \tag{2}$$

$$E_{GAP} = E_{LUMO} - E_{SOMO} \tag{3}$$

$$\eta = \frac{I - A}{2} = \frac{E_{LUMO} - E_{SOMO}}{2} \tag{4}$$

$$\sigma = \frac{1}{\eta} \qquad \qquad (5)$$

2.5. Biological tests

Antimicrobial tests were carried out using bacteria and fungi obtained from clinical samples. The microorganisms were *Staphylococcus aureus*, *Escherichia coli*, *Candida specie* and *Aspergillus niger*. The method by which these organisms were obtained was by plating out on selected solid medium. A small quantity of the samples from infected patient was streaked out on the selected medium from each isolates, i.e. mantol salt, tosine methylene blue agar, Sabouraud dextrose agar respectively. These isolates were sub-cultured into nutrient agar and Sabouraud dextrose agar for bacteria and fungi respectively. Specific biochemical tests were carried out for confirmation. Preparation of medium used for the antimicrobial assay: The Mueller Hinton agar used was prepared according to the manufacturer's specification, dissolved in appropriate volume of water and heat to gel on hot plate. The medium was sterilized by autoclaving at 121 °C for 15 minutes at 10 psi. Thereafter on cooling poured about 25 mL into sterile Petri dishes and left to set on the bench. Vapors were removed by drying in oven. Preparation of isolates used for this work: Four organisms were used which were *Staphylococcus aureus*, *E. coli*, *Candida sp.* and *Aspergillus niger*. Pure isolates were inoculated into broth medium and incubated for 18-24 hours. These were serially diluted to factor 3 using 10-fold dilution. These were carried out to standardize the number of cells inoculated into the medium for antimicrobial activity. The cells contain in the 0.5 mL that will be incubated will be equivalent to McFarland's standard. Seeding of Mueller Hinton agar plates with the test organism: 0.5 mL of each bacteria and fungi isolates were used to inoculate the medium based on the number of metal complex. A sterile spreader was used to spread the inoculum on the surface of the medium such that an even distribution of the isolates is obtained. Holes of 6 mm diameter were bored on the seeded plates based on the number of the complex fraction. Each hole was filled with the metal complex fraction such that each isolate has the different metal complex fraction (two concentrations were used C_1= 10 mg/ml and C_2= 20 mg/ml). As a control experiment, 40 mg·mL^{-1} of *Streptomycin* was used as standard for antimicrobial activity 100 mg·mL^{-1} of *Nystatin* was used as standard drug for fungi isolates. Plates were then incubated at 37 °C overnight. The zones around each disc were measured with a ruler.

3. Results and Discussion :

3.1. X-ray crystallographic study

Crystal Structures Description

The asymmetric unit of (**1**) consists of a discrete copper complex in which the metallic center is linked to three imidazole ligands through the three (N1A, N1B, N1C) nitrogen atoms and to a citrate molecule acting as a bidentate ligand through two oxygens; O6 belonging to the deprotonated α–carboxylato group and the hydroxyl oxygen O7, thus building a five-membered chelating ring. The ORTEP drawing of complex's (**1**) asymmetric unit is depicted in Figure 1.
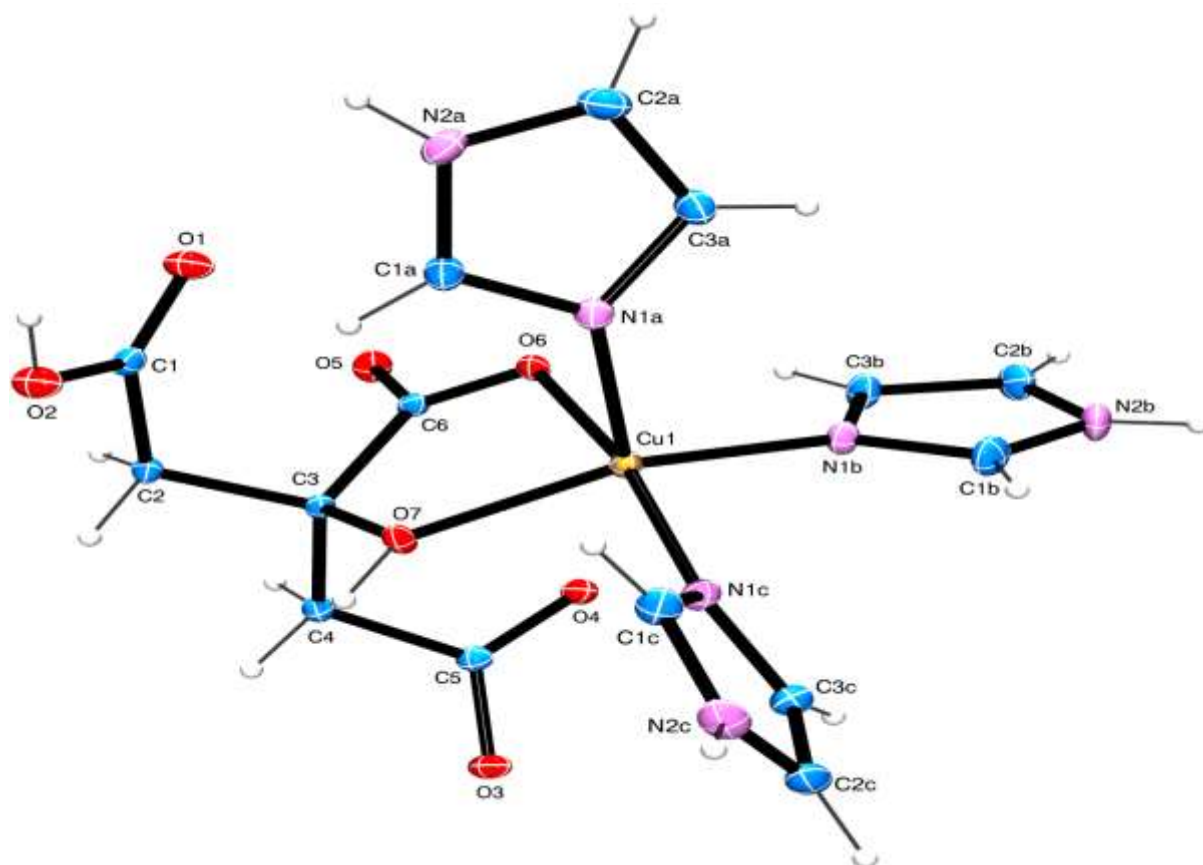
Figure 1. The Cu(II) coordination environment in the molecular structure of (**1**).

In order to describe the geometry of pentacoordinate complexes a degree of distortion is indicated by the τ value calculated according to the equation $\tau = (\beta - \alpha)/60$, with α and β being the two largest angles measured around the five-coordinated metallic centers. Therefore, an ideal square pyramid corresponds to a τ value of 0, while it equals 1 in perfect

trigonal bipyramidal geometry [30]. Thus, the τ value of 0.355 with α and β being 148.09(5) and 169.39(5)°, respectively, suggests that the Cu(II) ion in (**1**) adopts a geometry significantly distorted towards square pyramidal, with a N_3O_2 donor set in which the equatorial plane is occupied by the two citrate oxygens O6 and O7, and the two N1B and N1C nitrogens, with a bond distance Cu−O/N ranging from 1.9417(11) to 2.0563(11) Å. Whereas, in the apical position is situated the third imidazole N1A nitrogen, showing a longer bond distance of 2.1839(14) Å. The copper is 0.33 Å above the N_2O_2 plane towards the axially-coordinated N1A imidazole nitrogen. The distances are in the normal ranges and are consistent with those reported in similar imidazole-containing pentacoordinated copper(II) carboxylate structures; [Cu(im)$_2$(mal)]$_n$ [31], [Cu(H$_2$lac)$_2$(im)], [Cu(H$_2$mlac)$_2$(im)] [32] and [Cu(pydc)(H$_2$O)(4-meim)$_2$]·H$_2$O [33], where (im, mal, lac, mlac, pydc, meim) stands respectively for (imidazole, malonate, lactate, 2-methyllactate, pyridine-2,5-dicarboxylate, 4-methylimidazole). Summary of relevant bond lengths and angles is given in Table 2.

The asymmetric unit of (**2**) consists of a non-coordinating imidazolium cation and a mononuclear five-coordinated anionic copper(II) complex. The crystal structure reveals that the metallic centre is surrounded by two imidazole N1A and N1B nitrogen atoms and three tridentate-citrate oxygens; O1 belonging to one of the two deprotonated β−carboxylate groups, O7 which originates from the hydroxyl group and O5 arising from the α−carboxylate group. It should be mentioned that the Cu(II) ion builds with the citrate oxygens edge-fused five-membered and six-membered chelating rings. Figure 2 provides a perspective view of the asymmetric unit of complex (**2**).
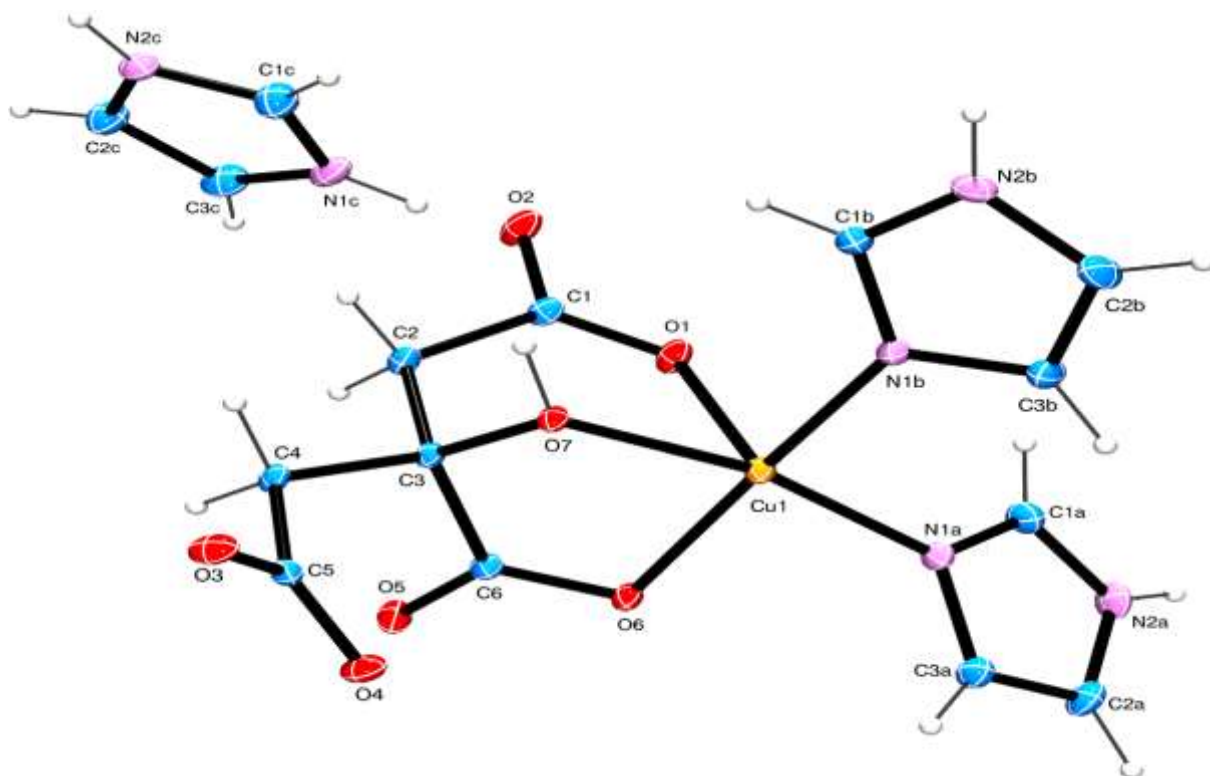
Figure 2. A view of the asymmetric unit of (**2**) showing the atom-numbering scheme and thermal displacement ellipsoids drawn at the 30% probability level.

By considering the two largest coordination angles within (**2**) (α and β being respectively 166.84(6) and 169.79(6)°), the geometry around the copper(II) ion is therefore best described as square pyramidal with a very small trigonal bipyramidal component τ of 0.049. The two N1A and N1B ligand nitrogen atoms and the two tridentate-citrate O6 and O7 oxygens are defining the equatorial positions of the CuN_2O_3 core. The Cu–O are in the ranges of 1.9474–2.0088(10) Å and the Cu–N bond distances fall in the range from 1.9657(14) to 1.9816 (14) Å. The axial position occupied by the third O1 citrate oxygen exhibits a Cu–O bond distance of 2.3082(13) Å. The copper is 0.146 ♦ above the N_2O_2 plane towards the axially-coordinated O1 citrate oxygen. The selected bond lengths and angles, listed in Table 2, are in agreement with the geometric parameters observed in other analogous imidazole complexes [34] and similar metallic citrate systems [35]. It is worth noting that the bond distances and angles arising from the two complexes (**1**) and (**2**) are very comparable except for the apical distance and the three angles involving the O7 hydroxyl oxygen (O–Cu1–O7, N–Cu1–O7 and O7–Cu1–N/O). Moreover, the imidazolium moieties show geometric parameters comparing well with the values described in other imidazolium containing salts; imidazolium fumarate [36],

imidazolium 4–nitrophenolate 4–nitrophenol monohydrate [37], imidazolium 3-carboxy-4-hydroxybenzenesulfonate [38], imidazolium 2,4-dihydroxybenzoate [39] and 2-methylimidazolium hydrogen maleate [40].

Table 2.

Selected bond distances and angles in (**1**) and (**2**).

	Complex (**1**)	Complex (**2**)
Bond lengths (Å)		
Cu1—O1	-	2.3082 (13)
Cu1—O6	1.9417 (11)	1.9474 (12)
Cu1—O7	2.0563 (11)	2.0088 (10)
Cu1—N1A	2.1839 (14)	1.9816 (14)
Cu1—N1B	2.0170 (13)	1.9657 (14)
Cu1—N1C	1.9842 (13)	-
Bond angles (°)		
O1—Cu1—O7	-	82.59 (4)
O6—Cu1—O1	-	90.15 (5)
O6—Cu1—O7	78.39 (4)	81.20 (4)
O6—Cu1—N1A	91.08 (5)	87.28 (5)
O6—Cu1—N1B	89.59 (5)	169.79 (6)
O6—Cu1—N1C	169.39 (5)	-
N1A—Cu1—O1	-	103.90 (6)
N1A—Cu1—O7	104.05 (5)	166.84 (6)
N1B—Cu1—O1	-	98.79 (6)
N1B—Cu1—O7	148.09 (5)	95.01 (5)
N1B—Cu1—N1A	105.63 (6)	95.27 (6)
N1C—Cu1—O7	92.54 (5)	-
N1C—Cu1—N1A	96.50 (6)	-
N1C—Cu1—N1B	95.47 (6)	-

The crystal structures of the two complexes are mainly dominated by supramolecular N–H···O hydrogen-bonding (Table 3). Each molecule of (**1**) is thus surrounded by seven other complex molecules (Figure 3a), bounded through four N–H···O intermolecular H-bonds, among which a chelated interaction involving the bifurcated imidazole N2B donor with the two deprotonated α–carboxylate O5 and O6 oxygens of the same citrate (x+1/2, -y+1/2, z+1/2) is observed [N2B—H2NB···O5, 3.060(2) ♦ and N2B—H2NB···O6, 2.8782(18) ♦].

These two interactions combine along the c-direction to build up infinite C(6) chains [41] connected together by means of the O7—H7···O3 hydrogen bond to produce bidimensional sheets in the (*bc*) plane. In addition, two moderate O–H···O hydrogen bonds, resulting from the interaction of the bifurcated deprotonated β−carboxylate O3 acceptor with the hydroxyl O7 oxygen [O7—H7···O3, 2.5860(15) ♦, (-*x*+2, -*y*, -*z*+2)] and the protonated β−carboxyl O2 atom [O2—H2···O3, 2.6894(18) ♦, (*x*-1, *y*, *z*)], come completing the complex molecules environment. It is worth to be mentioned that the O7—H7···O3 hydrogen bond delineate a symmetric $R^2_2(12)$ ring motifs. The three-dimensional hydrogen-bonding framework displays besides the contribution of four weak C–H···O and C–H···N interactions connecting the citrate C2 atom with the β−carboxyl O2 oxygen, and a carbon of each of the three imidazoles (C1A, C2B, C2C) with the (protonated carboxyl O2 atom, imidazole N1A nitrogen, protonated β−carboxyl O1 oxygen).

Table 3.

Hydrogen bonds geometry (Å, °) in (**1**) and (**2**).

D—H···*A*	*D*—H	H···*A*	*D*···*A*	*D*—H···*A*
Complex (**1**)				
O2—H2···O3^i	0.82	1.90	2.6894 (18)	161
C2—H2*D*···O1^{ii}	0.97	2.49	3.452 (2)	171
N2*A*—H2*NA*···O4^i	0.86	1.97	2.7997 (19)	161
N2*C*—H2*NC*···O4^{iii}	0.86	2.05	2.868 (2)	158
C1*A*—H1*A*···O2^{iv}	0.93	2.62	3.414 (2)	144
N2*B*—H2*NB*···O6^v	0.86	2.16	2.8782 (18)	141
N2*B*—H2*NB*···O5^v	0.86	2.26	3.060 (2)	155
C2*C*—H2*C*···O1^{vi}	0.93	2.56	3.276 (2)	134
C2*B*—H2*B*···N1*A*^{vii}	0.93	2.70	3.564 (3)	155
O7—H7···O3^{viii}	0.89	1.70	2.5860 (15)	171
Complex (**2**)				
N2*A*—H2*NA*···O2^{iv}	0.86	1.92	2.7778 (19)	172
N2*B*—H2*NB*···O4^i	0.86	1.89	2.7350 (19)	166
C1*B*—H1*B*···O3^{ix}	0.93	2.39	3.172 (2)	142
C3*A*—H3*A*···O4^x	0.93	2.47	3.388 (2)	168
C2*B*—H2*B*···O4^{ii}	0.93	2.45	3.362 (2)	167

C2—H2D···O3ⁱˣ	0.97	2.58	3.123 (2)	116
N1C—H1NC···O2	0.86	1.82	2.678 (2)	180
N2C—H2NC···O6ˣⁱ	0.86	2.62	3.1458 (19)	121
N2C—H2NC···O5ˣⁱ	0.86	1.84	2.6795 (19)	164
C3C—H3C···O1ˣⁱⁱ	0.93	2.34	3.222 (2)	159
O7—H7···O3ⁱˣ	0.88	1.63	2.5162 (16)	175

Symmetry codes: (i) *x*-1, *y*, *z*; (ii) -*x*+1, -*y*, -*z*+1; (iii) *x*, *y*, *z*+1; (iv) -*x*+1, -*y*, -*z*+2; (v) *x*+1/2, -*y*+1/2, *z*+1/2; (vi) *x*+1, *y*, *z*+1; (vii) *x*+1/2, -*y*+1/2, *z*-1/2; (viii) -*x*+2, -*y*, -*z*+2; (ix) -*x*+1, -*y*+1, -*z*+1; (x) -*x*+2, -*y*, -*z*+1; (xi) *x*-1, *y*+1, *z*; (xii) -*x*+1, -*y*, -*z*+2.
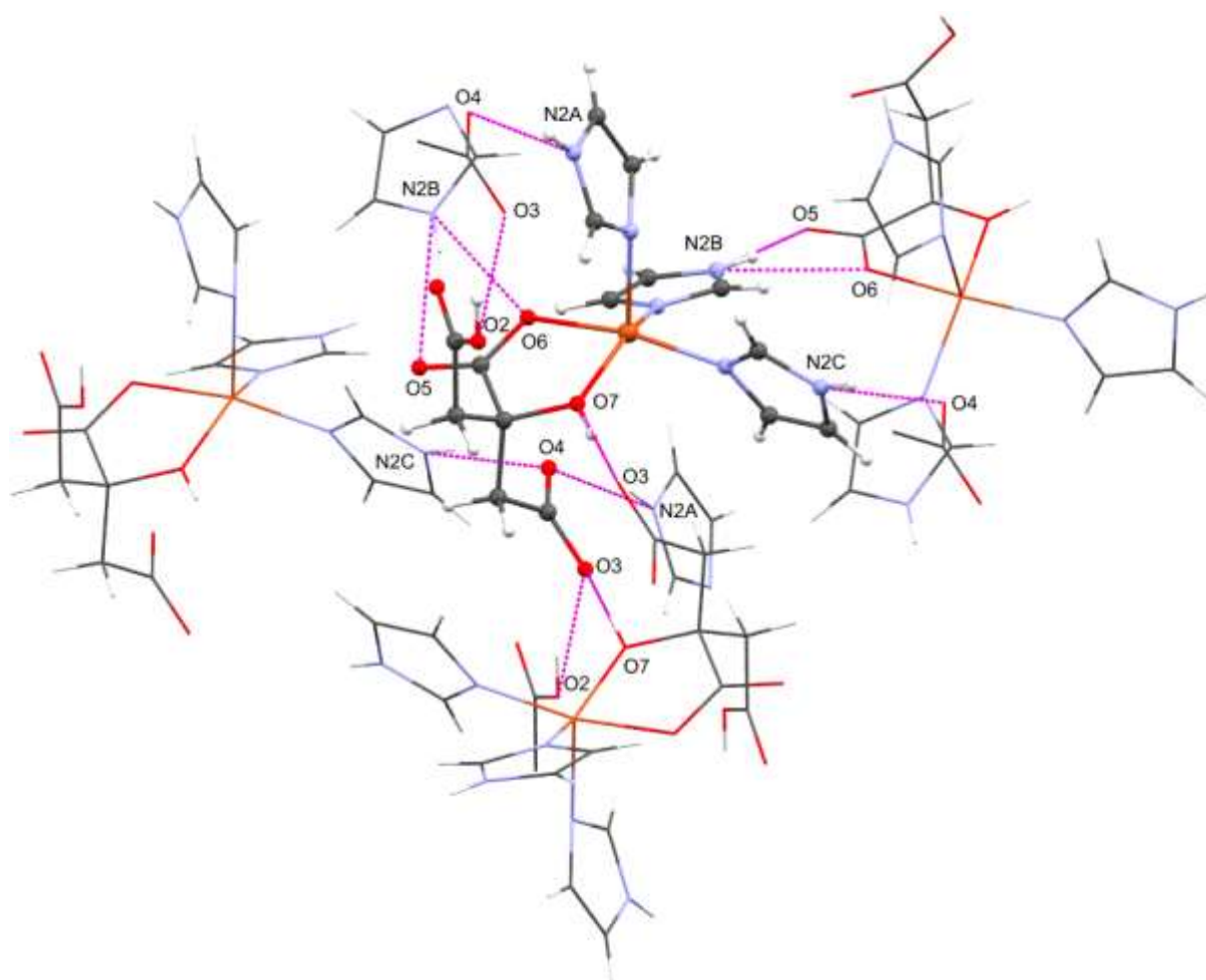
(a)
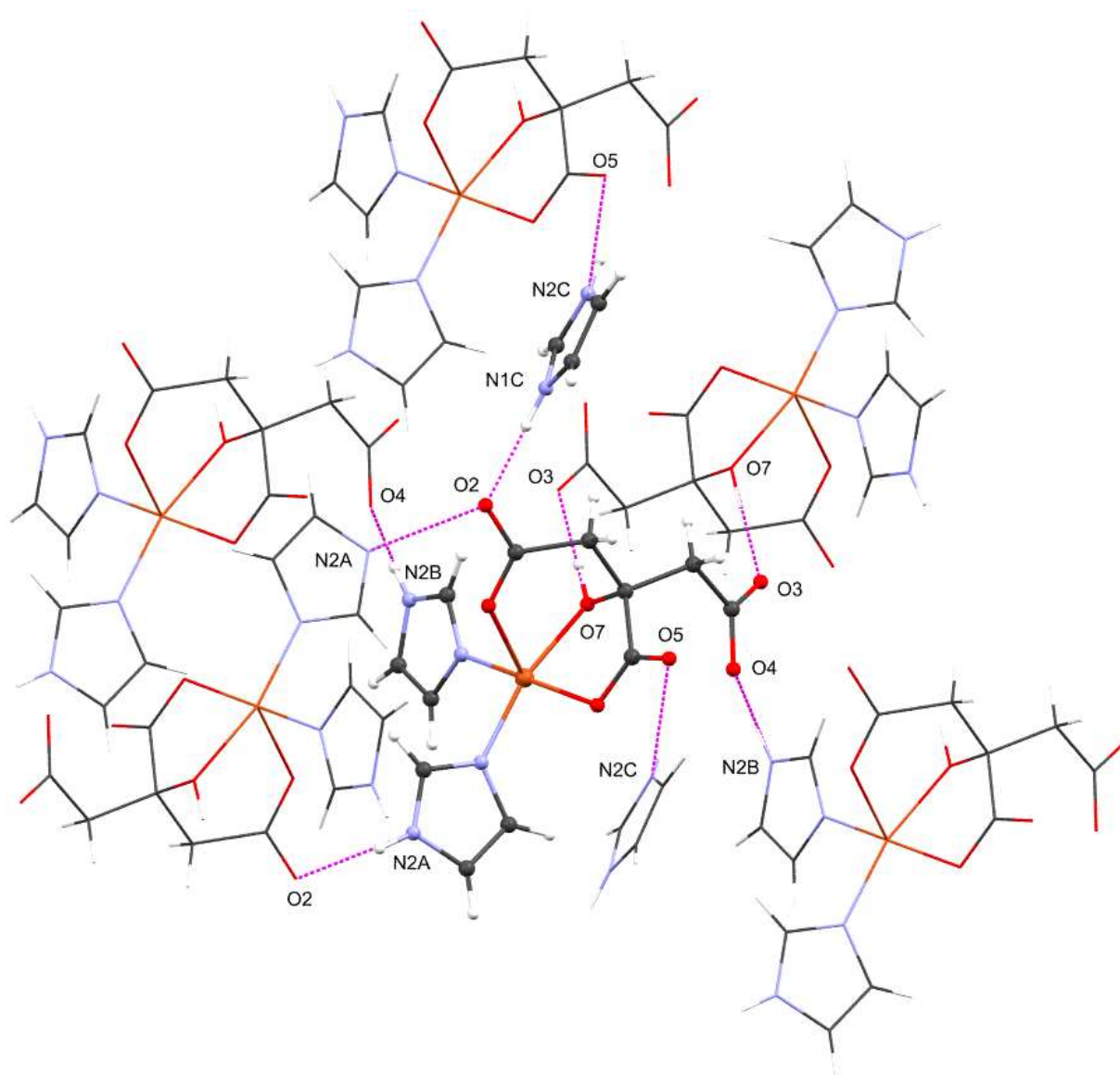
(b)

Figure 3. A perspective view of the neighboring environment surrounding the molecular units in the crystal structure of (a) (**1**) and (b) (**2**) linked by means of hydrogen bonds.

Likewise, compound (**2**) exhibits four complex neighbors and two uncoordinated imidazolium molecules in the immediate environment of each copper complex molecule. Whereas, the free imidazole moieties show only two complex molecules in their neighborhood (Figure 3.b). As a result, each molecule of the copper (II) complex is linked to its four complex neighbors through two moderate N–H···O hydrogen bonds (and their two reciprocal O···H–N interactions) involving the two N2A and N2B nitrogen atoms with the two deprotonated β−carboxylate O2 and O4 oxygens [N2A—H2NA···O2, 2.7778(19) ♦, (-x+1, -y, -z+2) and N2B—H2NB···O4, 2.7350(19) ♦, (x-1, y, z)]. This connection is as well assured *via* the O–

H···O interaction (and its reciprocal O···H–O) between the hydroxyl O7 oxygen and the β–carboxylate O3 atom [O7—H7···O3, 2.5162(16) ♦, (-x+1, -y+1, -z+1)], which combine together, as in (**1**), to build dimeric complex moieties described as $R_2^2(12)$ graph-set rings. Moreover, each complex molecule is bounded to two imidazolium *via* its β–carboxylate O2 oxygen and the imidazolium N1C atom. The α–carboxylate group displays additionally a chelate bond through both O5 and O6 oxygens together with the imidazolium N2C nitrogen, resulting thus in one moderate and one weak N–H···O hydrogen bonds (Table 3). Compound (**2**) shows infinite [41] chains of complex molecules stabilized basically by the N2B—H2NB···O4 interaction which define a C(10) descriptor. These chains are further linked together *viz* N2A—H2NA···O2 and O7—H7···O3 to end up in infinite sheets growing parallel to the (*ac*) plane. Similarly to (**1**), weak C–H···O intermolecular forces are contributing to stabilize the three-dimensional hydrogen-bonding networks in (**2**), however no C–H···N interactions have been observed.

Hirshfeld Surface analysis

Hirshfeld surface analysis [42] represents an appealing approach to the investigation of the different contacts between molecules in crystals. It has proven to be a useful tool for the analysis and visualization of intermolecular interactions and therefore the crystal packing behavior of molecules, particularly for the purpose of features comparison in given compounds. It is furthermore of interest to analyze the intermolecular interactions present in the crystal packing in terms of a bi-dimensional visualization of d_e and d_i based on decomposition of the *Hirshfeld* surfaces into contributions from the different contacts and generated as a 2D-fingerprint plot [43]. The different properties mapped on the *Hirshfeld* surfaces and the fingerprint plots were generated using *CrystalExplorer* 3.1 [44]. The relative contributions of the different interactions of compounds (**1**) and (**2**) to the global *Hirshfeld* surfaces (Scheme 1) are given as full and decomposed 2D-finger plots, and are illustrated in Figure 4.
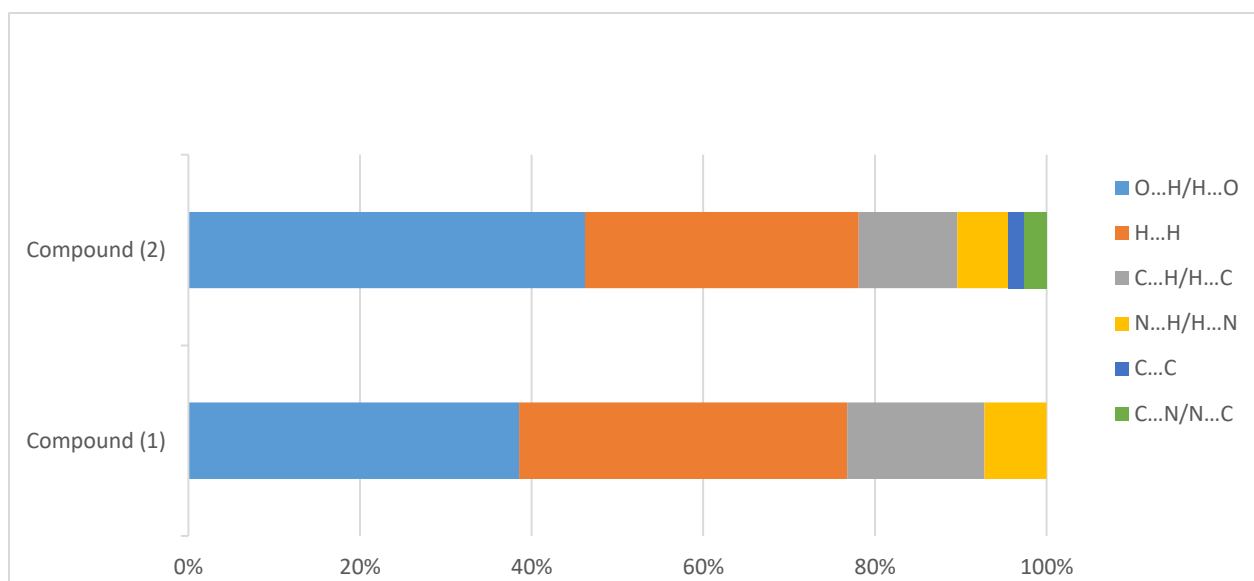
Scheme 1. Relative contributions of intermolecular contacts to the *Hirshfeld* areas in (**1**) and (**2**).

(a) **(b)**
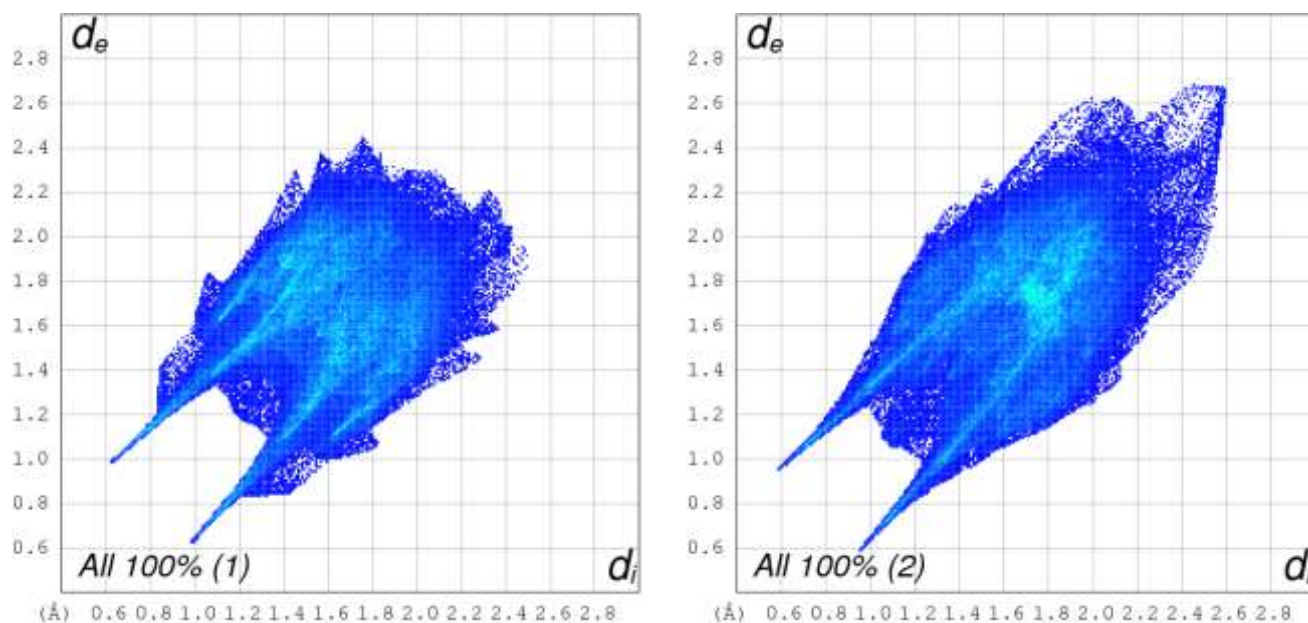
Figure 4. (a), (b) Full 2D-fingerprint plots in (**1**) and (**2**).

The finger prints of both compounds exhibit contribution similarity of the different intermolecular contacts except for the O···H/H···O contacts, considered as the most dominant and appearing as a pair of sharp symmetric spikes (Figures S1a and S1b), which appear to be

more significant (45.4%) over the total *Hirshfeld* surface around (**2**) compared to (**1**), being only of 37.8%. Nevertheless, these contacts could be attributed in both compounds to the intermolecular O–H···O, N–H···O and C–H···O hydrogen-bonding interactions, and show prominent long spikes at ($d_e + d_i = 1.6$ ♦) for (**1**) and at ($d_e + d_i = 1.55$ ♦) for (**2**), resulting from the strong reciprocal interactions O7–H7···O3/O3···H7–O7. This is reflected by the presence of the two large red spots over the d_{norm} surface defined by features (1) and (9) in (Figures 5a and 5b), whereas the small red dots (features (8) for compound (**1**) in Figure 5a) represent the weak C–H···O/O···H–C hydrogen bonds, considering that the spot size and color depends on the interaction strength.

(a)
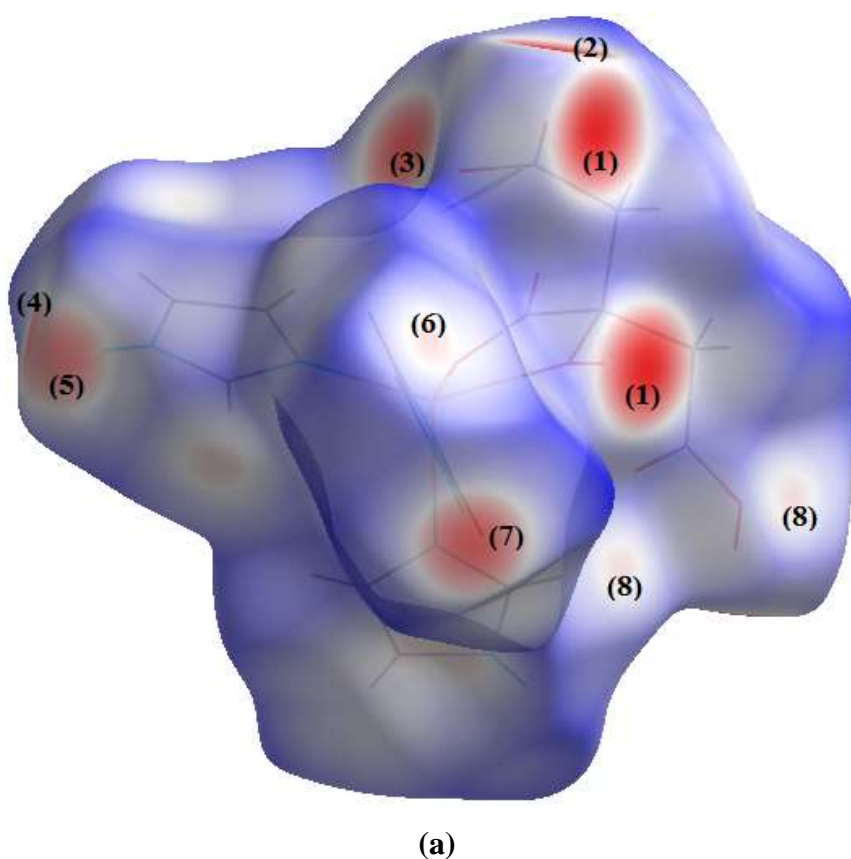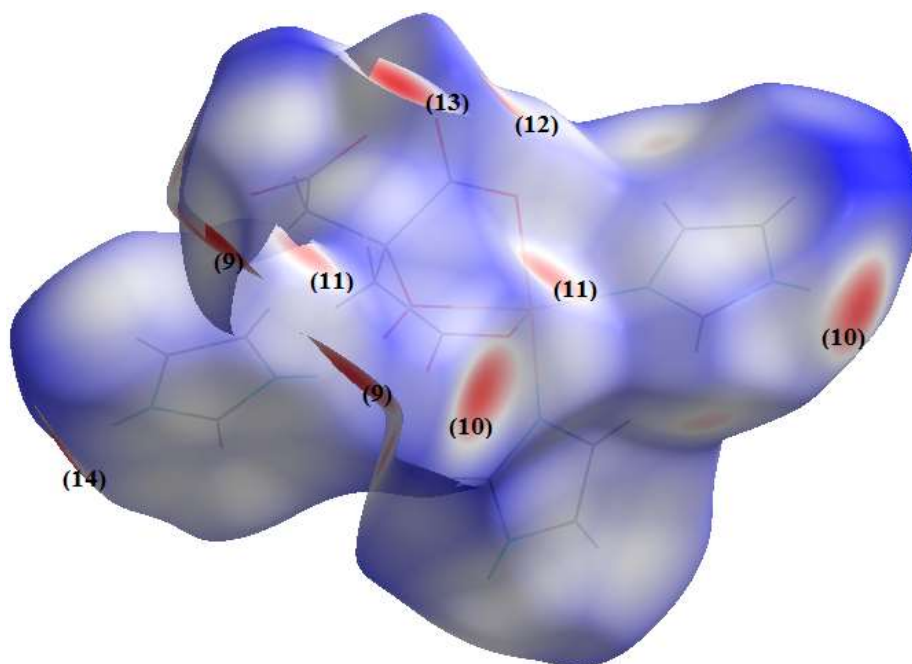
(b)

Figure 5. d_{norm} property mapped on the *Hirshfeld* surfaces of compounds (**1**) and (**2**). (a) The features (1), (2), (3), (4), (5), (6), (7) and (8) describe the interactions O7–H7···O3/O3···H7–O7, O3···H2–O2, O4···H2NA–N2A, N2B–H2NB···O5, N2B–H2NB···O6, C1A–H1A···O1, N2C–H2NC···O4 and C1A–H1A···O2/O2···H1A–C1A. (b) The following features (9), (10), (11), (12), (13) and (14) define the interactions O7–H7···O3/O3···H7–O7, N2A–H2NA···O2/O2···H2NA–N2A, C3C–H3C···O1/O1···H3C–C3C, O5···H2B–C2B, O4···H2NB–N2B and O5···H2NC–N2C, respectively.

The scattered points covering a large region of the two-dimensional maps arise from the H···H contacts and are observed to be the second highest contributor towards the total *Hirshfeld* areas (Figures S1c and S1d), with a contribution of 37.5 % and 31.3 % for (**1**) *vs.* (**2**). As it can be seen from the two figures, the shortest contacts observed at about ($d_e = d_i \sim$ 1.19 $\blacklozenge$) and ($d_e = d_i \sim$ 1.08 $\blacklozenge$) are associated to the non-classical interactions C2–H2E···H1A–C1A and C4–H4A···H1A–C1A, respectively. Whereas, the C···H/H···C contacts appearing as wings in the 2D-histograms (Figures S1e and S1f) are less significant and thus represent 15.7 % and 11.3 % from the whole histograms of (**1**) and (**2**), respectively. The two wings show limits at ($d_e + d_i \sim$ 2.62 $\blacklozenge$) and ($d_e + d_i \sim$ 2.54 $\blacklozenge$) resulting from shortest contacts which could be related to N–H···π and C–H···π interactions, respectively, involving

the imidazole (N2B, C1A) atoms in (**1**) and (C1A, C3C) carbons in (**2**). Moreover, there are 7.1 % and 5.9 % participations to the global areas of (**1**) and (**2**) coming from the N···H/H···N contacts, as it is shown in Figures S1g and S1h, and more precisely the two shortest interactions C2B–H2B···N2A and C2C–H2C···N2A appearing at ($d_e + d_i$ ~ 2.55 ♦) and ($d_e + d_i$ ~ 2.68 ♦). A final observation deriving from the molecular environment description by considering the fingerprint plots concerns the relative areas associated with the C···C and N···C/C···N contacts given in Figures S2a and S2b, and associated with the planar π···π stacking arrangement and lp···π/π···lp interactions in compound (**2**). In fact, from the two Figures, it can be seen that less than 3 % of the surface is identified as N···C/C···N contacts, whereas the C···C forces are less frequent with around 2 % of the entire molecular surface. These numbers are supported by the appearance of red and blue triangles on the shape-indexed surface of (**2**) and identified with black arrows in Figure 6.

It is worth to be noted that this is compensated in (**1**) by the observation of around 2 % of the total *Hirshfeld* area, resulting equally from the contribution of O···O and O···C/C···O contacts which are associated to the presence of lp···lp and lp···π/π···lp interactions.
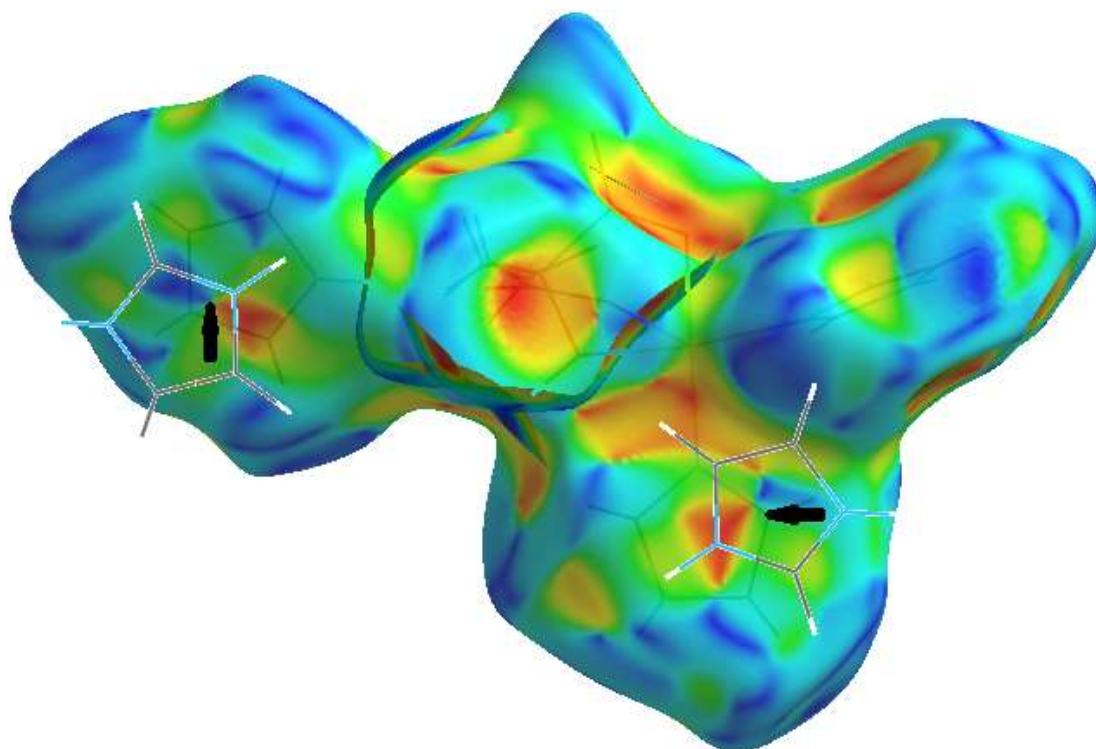
Figure 6. Shape-index property mapped on the *Hirshfeld* surface around (**2**).

In addition, the *Hirshfeld* surfaces associated to compounds (**1**) and (**2**) have been displayed with the *MoProViewer* software [45] and colored according to the values of the atomic number of the atoms contributing most to the local electron density (Figures 7b and 7e) in order to highlight the chemical type of the closest interacting atoms in the crystal surrounding (Figures 7c and 7f).

(a)

(b)

(c)

(d)

(e)   **(f)**
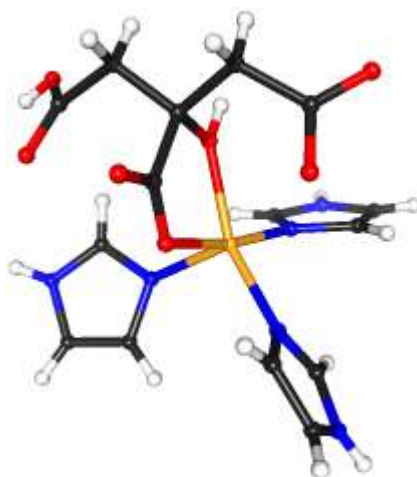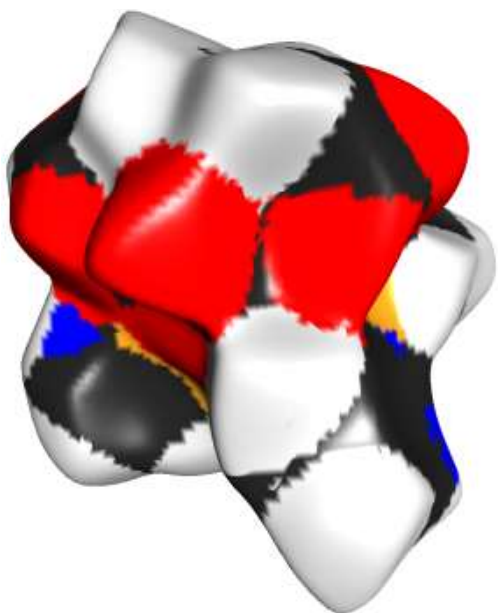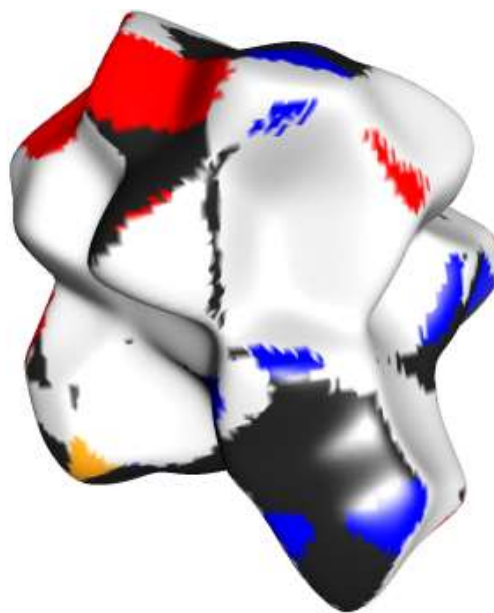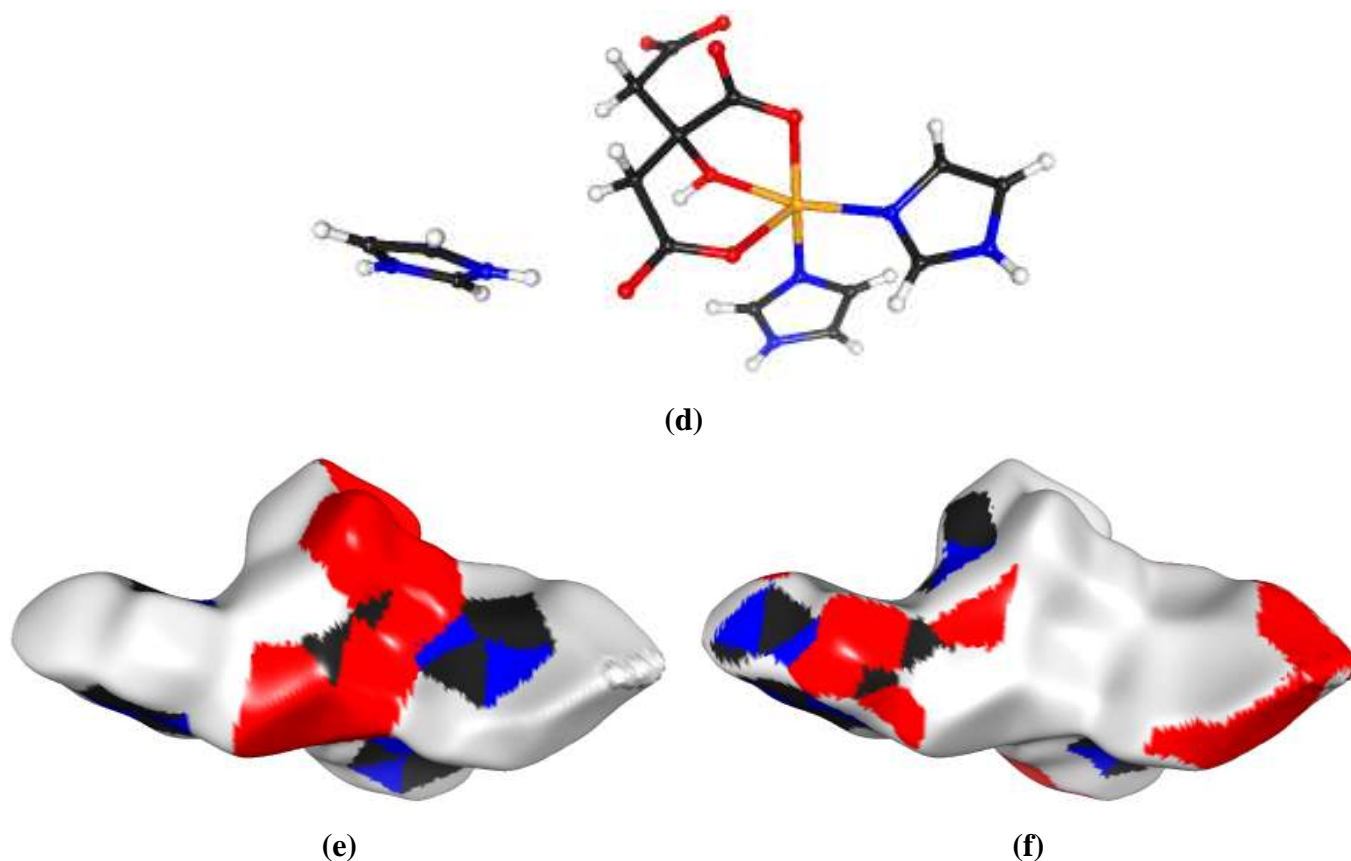
Figure 7. (a), (d) Orientation of the molecules of (**1**) and (**2**). *Hirshfeld* surfaces around the asymmetric units of (**1**) and (**2**) colored according to the (b), (e) internal or (c), (f) external atoms contributing most to the electron density.

Enrichment ratio

The intermolecular interactions in (**1**) and (**2**) were further evaluated by computing the enrichment ratios (*E*) [46], in order to examine the likelihood of two chemical species in the two complexes to be in contact and therefore to form intermolecular interactions with themselves and with the other species. The proportion of actual contacts in the crystal structures of (**1**) and (**2**), the theoretical proportion of random contacts and the related enrichment ratios are given in Table 4.

Table 4.

Percentages of *Hirshfeld* surface contacts, derived random contacts and enrichment ratios for the different chemical species in (**1**) and (**2**).

	(1)					(2)				
	H	O	N	C	Cu	H	O	N	C	Cu
Contacts (C, %)[a]										
H	37.5	–	–	–	–	31.3	–	–	–	–
O	37.8	0.9	–	–	–	45.4	0.1	–	–	–
N	7.1	0.0	0.0	–	–	5.9	0.0	0.5	–	–
C	15.7	0.9	0.0	0.0	–	11.3	0.1	2.6	1.7	–
Cu	0.0	0.0	0.0	0.0	0.0	0.5	0.0	0.0	0.7	0.0
Surface (S, %)										
	67.8	20.3	3.6	8.3	0.0	62.9	22.9	4.8	9.1	0.6
Random contacts (R, %)										
H	46.0	–	–	–	–	39.6	–	–	–	–
O	27.5	4.1	–	–	–	28.8	5.2	–	–	–
N	4.9	1.5	0.1	–	–	6.0	2.2	0.2	–	–
C	11.3	3.4	0.6	0.7	–	11.4	4.2	0.9	0.8	–
Cu	0.0	0.0	0.0	0.0	0.0	0.8	0.3	0.1	0.1	0.0
Enrichment (E)[b]										
H	0.82	–	–	–	–	0.80	–	–	–	–
O	1.37	0.22	–	–	–	1.58	0.02	–	–	–
N	1.45	0.00	–	–	–	0.98	0.0	–	–	–
C	1.39	0.26	–	–	–	0.99	0.02	2.89	–	–
Cu	–	–	–	–	–	–	–	–	–	–

[a] The contacts proportions are obtained from the *CrystalExplorer* software [44].

[b] The enrichment ratios are not computed for the random contacts lower than 0.9 % as they are not meaningful [46].

For pairs of elements with a higher propensity to form contacts the enrichment ratio is larger than unity, while its values are lower than unity for pairs tending to avoid contacts. Therefore, the H···H contacts in the two compounds are slightly under-represented with an enrichment ratio E_{HH} of about 0.80 in both cases. Though, being enriched with $E_{HO} = 1.58$ the O–H···O, N–H···O and C–H···O hydrogen bonds appear to be the driving forces in the crystal packing of (**2**) compared to (**1**) which show a lower enrichment of 1.37. On the other hand, the H···N and H···C contacts are over-represented in (**1**) in comparison to (**2**) with $E_{HO/N}$ values of 1.37 and 1.45 respectively (for only unity in the case of (**2**)), thus showing a high propensity to

form C–H⋯N, C–H⋯π and related interactions, as proved by means of the *Hirshfeld* surface analysis. It is to be noted that the formation of extensive π⋯*lp* interactions in (**2**) is reflected in the relatively high value of E_{CN} being equal to 2.89, while its propensity (**1**) is absolutely insignificant. Whereas, the C⋯O and O⋯O contacts are in the two cases very impoverished with $E_{OC/O} < 0.3$ in (**1**) and equal to 0.02 in (**2**). Moreover, the other XY contacts and self-contacts involving nitrogen, carbon and copper are completely avoided. Figure 8 exhibits the *Hirshfeld* surfaces built around (**1**) and (**2**), and displayed according to the different contact types and their proportions.
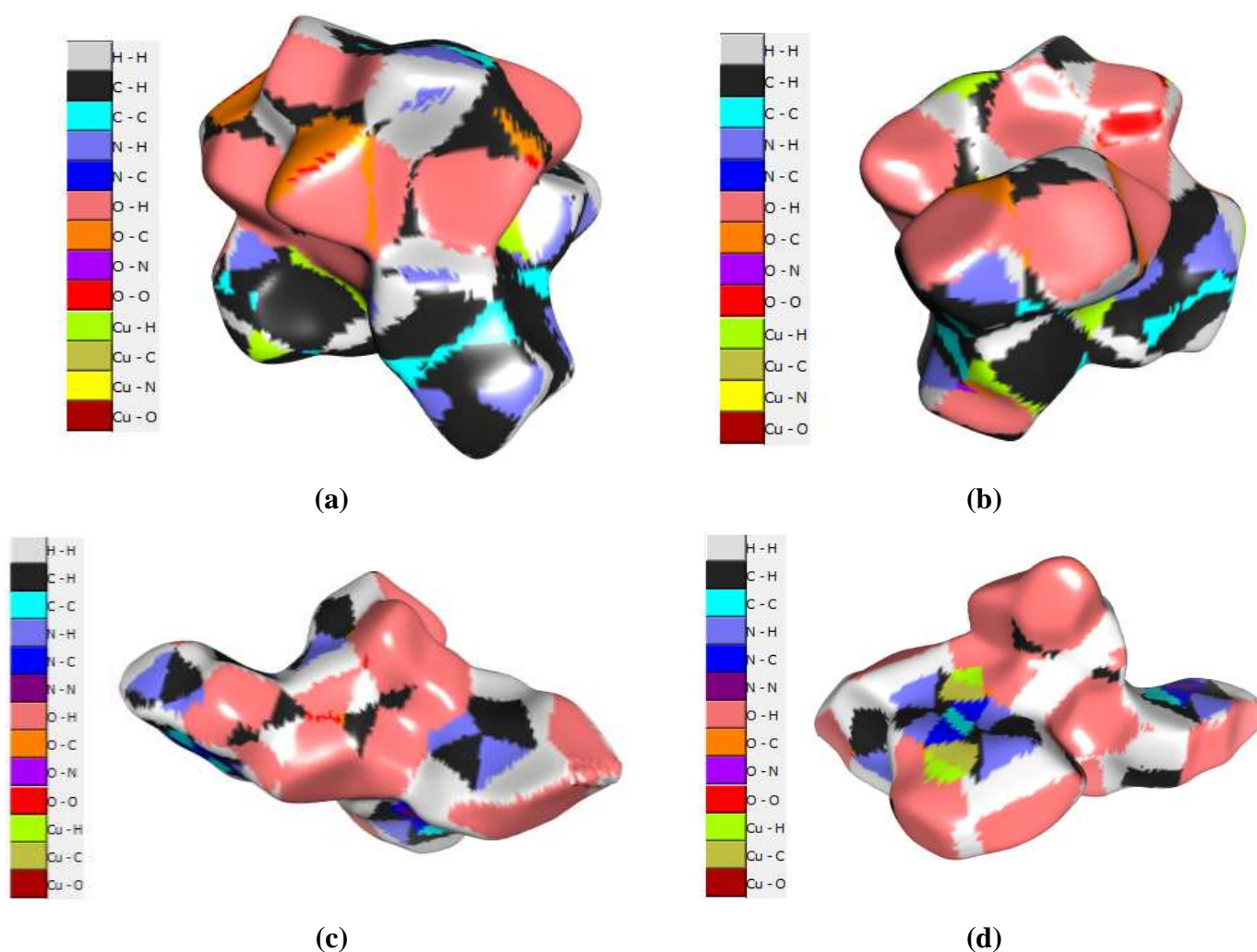
Figure 8. (a), (c) Front and (b), (d) back views of the *Hirshfeld* surfaces colored following the different contacts nature in (**1**) and (**2**).

Topological analysis

Topological description of the crystal structures could be undertaken by finding simple nets models [47] that usually ignore the geometrical parameters of an atomic array and rather focus on the overall structure connectivity [48]. For this purpose, and according to a topological analysis using *ToposPro* program [49], the three-dimensional hydrogen-bonding frameworks observed in (**1**) and (**2**) could be described as simplified nodal nets. Consequently, the entire assembly of (**1**) can be simplified to a **sev** (*sqc*44) uninodal (7)-connected underlying net (Figure 9) having the Schläfli symbol $\{4^{17}.6^4\}$, in which the nodes are the mass centers of the copper complex molecules and the connections between them are made of edges that mimic the hydrogen-bonding patterns made of two O–H···O and four N–H···O interactions.

(a)

(b)   **(c)**
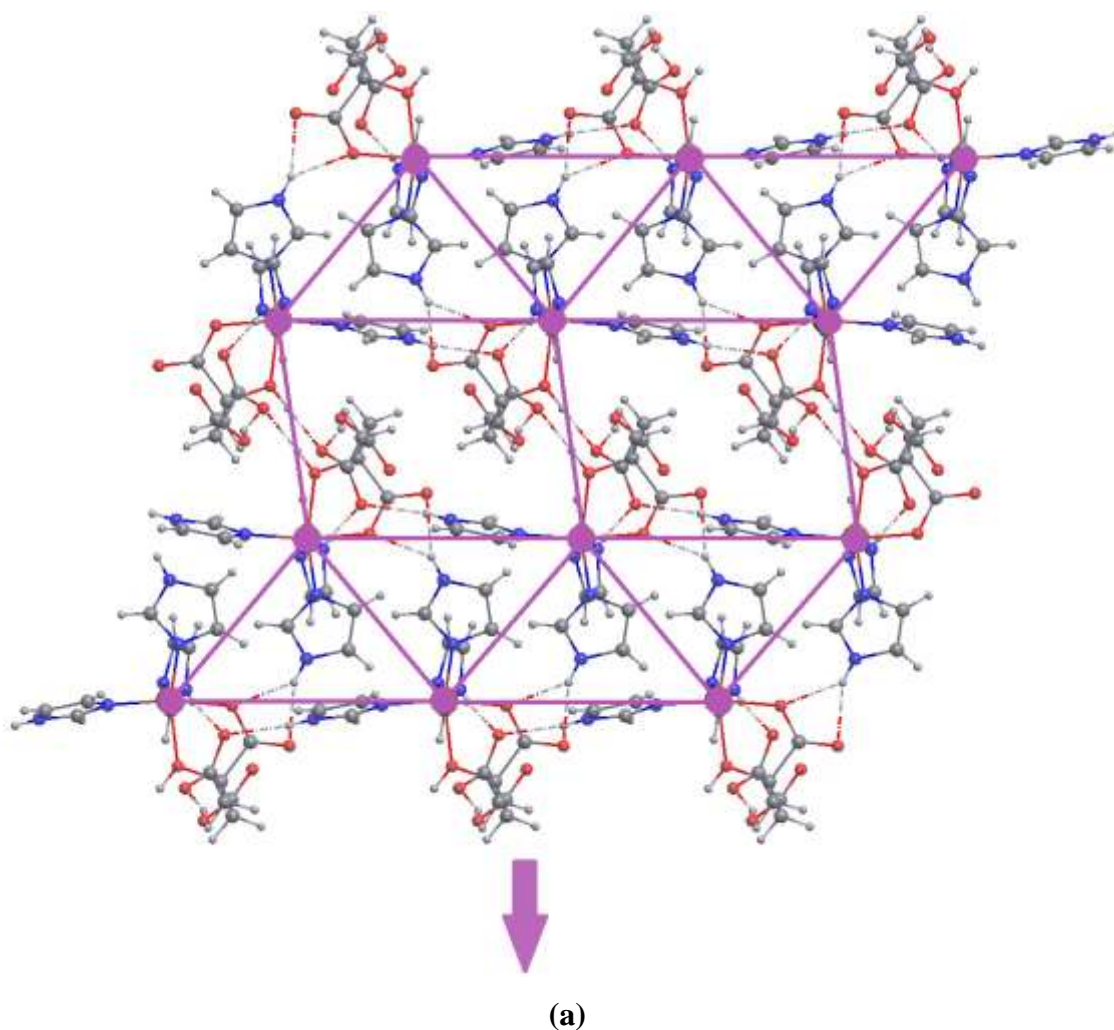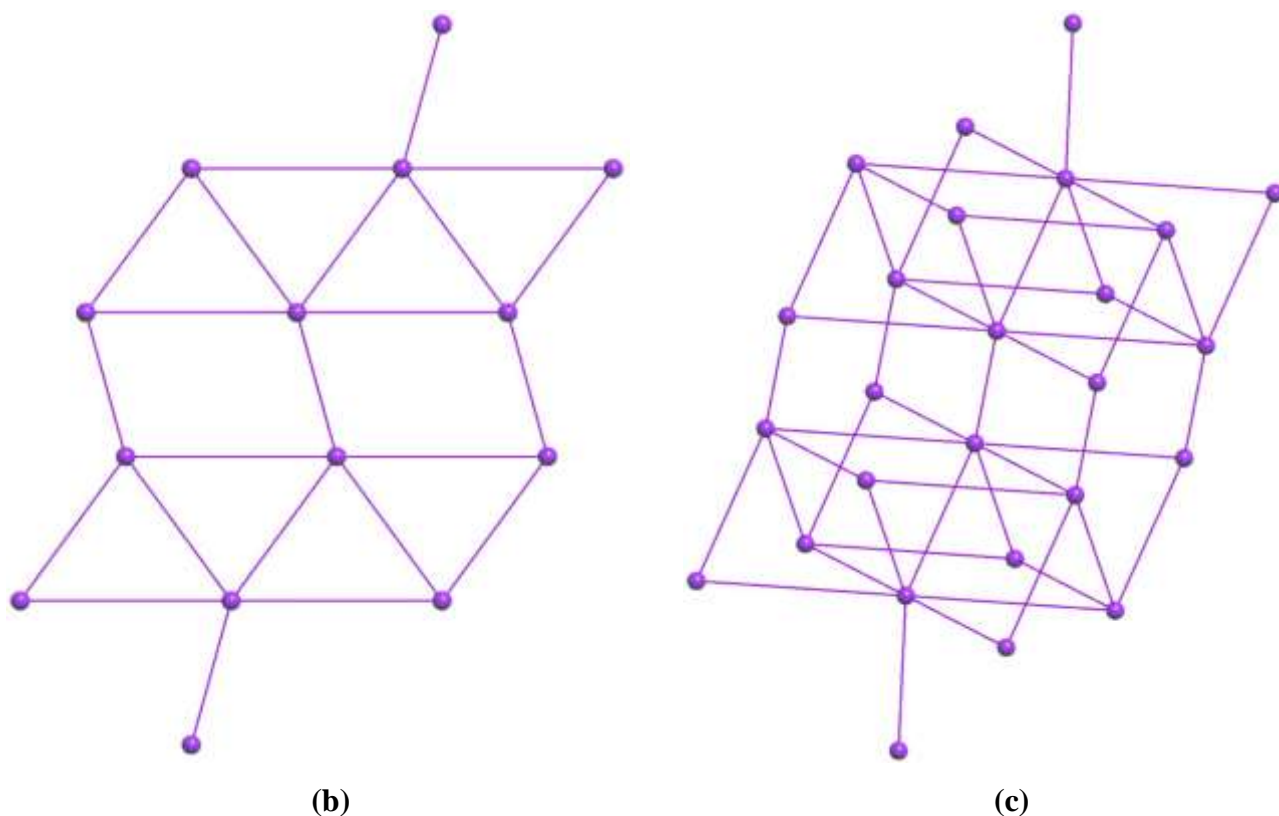
Figure 9. (a) Crystal packing of (**1**) showing the connectivity of each molecule through the hydrogen-bonding frameworks. Standard representation of the crystal structure of (**1**) given (b) along (100) and (c) in a perspective view. The corresponding underlying net is a 7-coordinated **sev.**

From a topological point of view, the copper complex molecules in (**2**) serve as 4-coodinated nodes, bonded to two other complex molecules and two free imidazole moieties (Figure 10). Whereas the imidazolium cations could be represented as 2-connected nodes which guarantee the link between two different complex molecules, by means of two N–H···O interactions. The two types of nodes are further interconnected through edges built of the different H-bonds present in the crystal structure, and the resulting 3D-framework is thus a (2,6)-connected binodal net with a unique $\{4^4.6^{10}.10\}\{6\}$ topology.
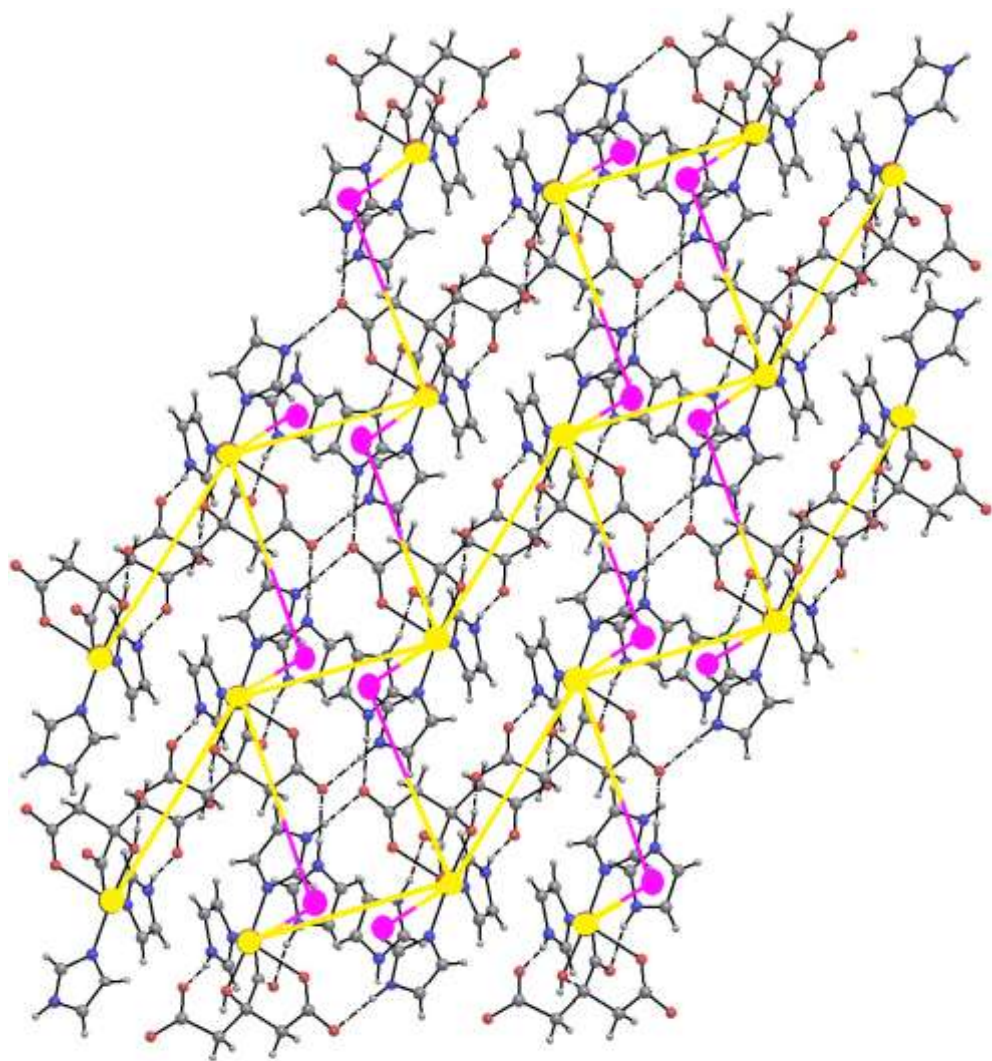
(a)
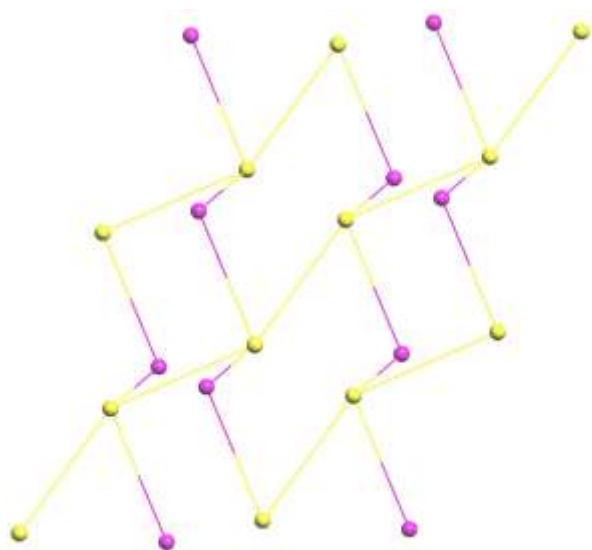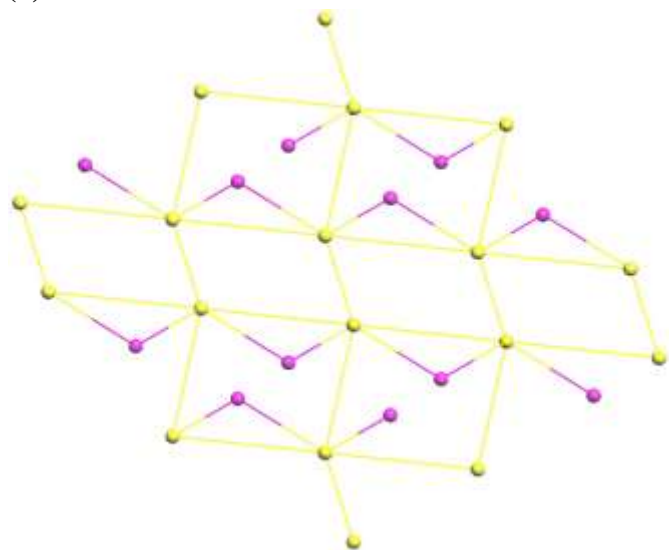
(b)   **(c)**

Figure 10. (a) Connectivity of the complex molecules and the imidazolium cations in (**2**). Views of the resulting (2,6)-c binodal 3D-network along the (b) [100] and (c) [010] directions.

If we consider that the bridging imidazolium cations (2-coordinated purple nodes) could be merged to the 6-connected nodes (yellow nodes) and contracted to edges, then a secondary simplification should be additionally applied to obtain the standard representation. Therefore, the previously obtained network could simplify further to a 6-connected uninodal primitive cubic lattice **pcu** (*sqc*1) underlying net with a point symbol of $\{4^{12}.6^{3}\}$ (Figure 11).

| (a) | (b) |
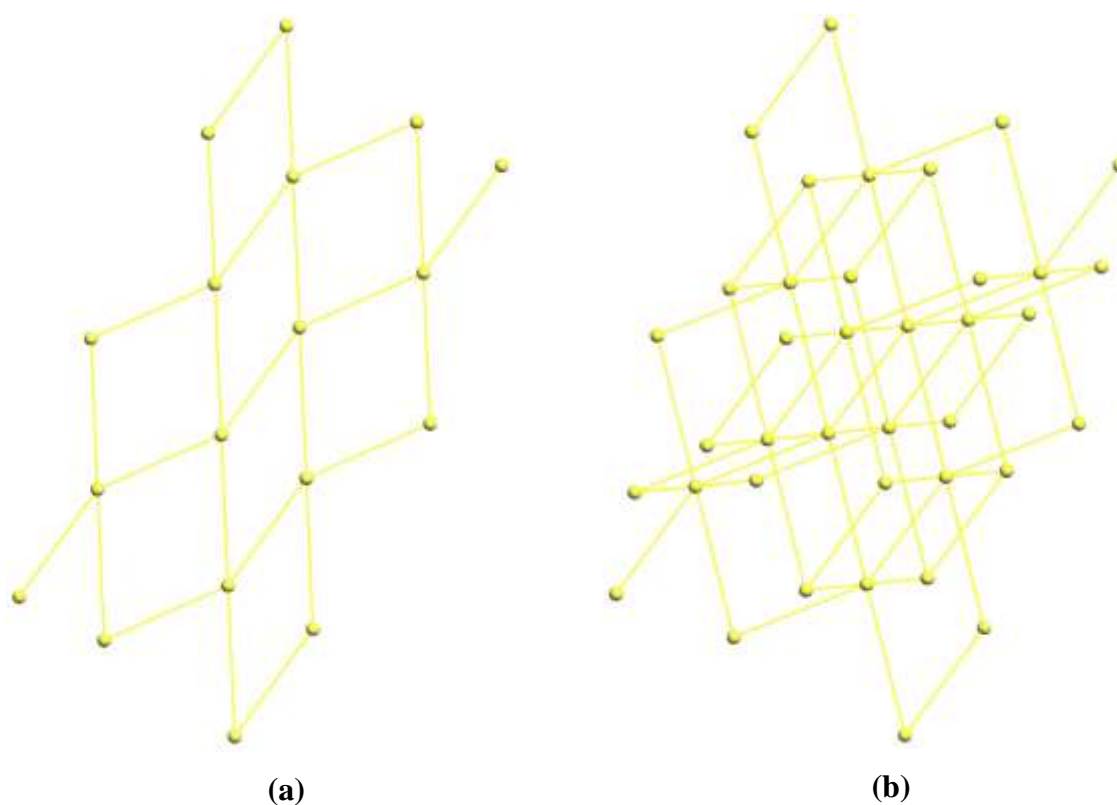
Figure 11. Views (a) along [100] and (b) in perspective of the simplified underlying net for the structure of (**2**), belonging to the **pcu** topology.

3.2. *Computational Results*
Optimized structures

The quantum HF computational analysis was performed to gain a better insight into the electronic and vibrational properties of the two mixed-ligands copper(II) complexes. Calculated structures of the complexes are represented in Figures S3a and S3b. Some relevant theoretical structural parameters in comparison to the experimental ones are given in Table 5.

As it can be noticed from Table 5, the calculated bond lengths and bond angles in complexes (**1**) and (**2**) were found to be approximately similar to the experimental data obtained by the X-ray crystallographic studies, suggesting a square pyramidal geometry for the two structures as it was confirmed from the crystal structures with τ values of 0.216 and 0.095. However, a slight deviation has been observed especially in the (Cu1—N1B, Cu1—O7) bonds of (**1**) and the (Cu1—O1, Cu1—O7) bonds in (**2**).

Table 5.

Comparative experimental and calculated structural parameters of the two copper complexes.

	Bond Lengths (Å)			Bond Angles (°)	
	Experimental	Calculated		Experimental	Calculated
For Complex (**1**)					
Cu1—N1A	2.184	2.149	N1A—Cu1—N1B	105.6	103.8
Cu1—N1B	2.017	2.304	N1A—Cu1—N1C	96.5	90.8
Cu1—N1C	1.984	2.149	N1A—Cu1—O6	91.1	87.8
Cu1—O6	1.942	1.946	N1A—Cu1—O7	104.1	97.7
Cu1—O7	2.056	2.643	N1B—Cu1—N1C	95.5	96.3
-	-	-	N1B—Cu1—O6	89.6	96.1
-	-	-	N1B—Cu1—O7	148.1	154.5
-	-	-	N1C—Cu1—O6	169.4	167.5
-	-	-	N1C—Cu1—O7	92.5	96.8
-	-	-	O6—Cu1—O7	78.4	71.1
For Complex (**2**)					
Cu1—N1A	1.982	2.153	N1A—Cu1—N1B	95.3	92.8
Cu1—N1B	1.966	2.141	N1A—Cu1—O1	103.9	176
Cu1—O1	2.308	1.946	N1A—Cu1—O6	87.28	87.1
Cu1—O6	1.947	1.929	N1A—Cu1—O7	166.8	93.5
Cu1—O7	2.009	2.388	N1B—Cu1—O1	98.8	84.8
-	-	-	N1B—Cu1—O6	169.8	170.3
-	-	-	N1B—Cu1—O7	95	112.5
-	-	-	O1—Cu1—O6	90.2	95.6
-	-	-	O1—Cu1—O7	82.6	85
-	-	-	O6—Cu1—O7	81.2	77.1

Spectral Analyses

The calculated IR spectra of both compounds are obtained at HF/6-31G(d)(LANL2DZ) level in gas phase and depicted in Figures S4a and S4b. Some stretching frequencies are given in Table 6 and are very comparable in both complexes, showing a stretching vibration mode of the (O–H) bonds at 4000 cm^{-1}. In addition, the absorption bands of the $\nu(N–H)$ stretching were calculated at 3900 cm^{-1}.

Table 6.

Stretching vibrations and related frequencies (cm^{-1}) in the calculated IR spectra of the complexes.

Vibration mode	Frequency	
	Complex (**1**)	Complex (**2**)
ν_{OH}	4047	4070
ν_{NH}	3911	3914
$\nu_{CH_{Aromatic}}$	3492	3488
$\nu_{CH_{Aliphatic}}$	3182	3158
$\nu_{C=O}$	1938	1909
$\nu_{C-C}, \nu_{C=O}$	1512	1544

Chemical shift values of carbon and hydrogen atoms in the ^{1}H and ^{13}C NMR spectra of the imidazole complexes are calculated by considering the TMS and given in Table 7. Chemical shift values of the aromatic carbon atoms are in the range of 109 – 147 ppm in (**1**) and 109 – 145 ppm in (**2**). Moreover, the citrate carbon signals appear from 41 to 168 ppm and from 45 to 177 ppm, in (**1**) and (**2**) respectively. Whereas, the values of the corresponding proton signals in the aromatic rings are in the range of 5.6 – 11.5 ppm for (**1**) and in the range of 5.3 – 8.2 ppm for (**2**), and the values 1.2 – 2.8 ppm were obtained for the hydrogen atoms connected to the aliphatic carbons for the two complexes.

Table 7.

^{1}H and ^{13}C NMR results for (**1**) and (**2**), calculated at the same level of theory.

	^{1}H NMR				^{13}C NMR	
	(**1**)	(**2**)			(**1**)	(**2**)
H2D	2.77	2.09	**C1**		166.95	176.54
H2E	2.49	1.20	**C2**		41.18	44.74
H4A	1.17	2.00	**C3**		66.55	71.25
H4B	1.72	2.81	**C4**		41.44	48.09
H2	5.25	-	**C5**		168.16	159.86
H7	11.18	6.15	**C6**		163.89	166.51
H1A	9.39	7.38	**C1A**		143.86	144.78
H2A	6.51	5.25	**C2A**		110.11	121.19
H3A	6.06	6.15	**C3A**		121.35	108.76
H1B	11.48	8.23	**C1B**		147.03	145.46
H2B	7.93	6.22	**C2B**		112.49	108.45
H3B	10.01	6.25	**C3B**		128.29	122.22
H1C	5.93	-	**C1C**		138.07	-
H2C	6.15	-	**C2C**		109.45	-
H3C	5.55	-	**C3C**		121.71	-
H2NA	7.38	6.85	**-**		-	-
H2NB	8.60	6.83	**-**		-	-
H2NC	6.68	-	**-**		-	-

Molecular Electrostatic Potential Maps

Molecular electrostatic potential (MEP or ESP) maps are important to investigate and analyze the sites of unusual electrostatic features corresponding to functionally important regions in the two molecular structures. For this purpose, the MEP maps of the two copper complexes were generated and represented in Figures 12a and 12b. In these maps, electronically rich regions are mainly colored in red or yellow, while highly positive electrostatic potential sites are attributed to the blue features on the two maps. Therefore, blue regions are dominant around the hydrogen atoms in (**1**) and (**2**), while the red regions appearing around the oxygen atoms show that they are the most electronegative sites of the two structures and are thus appropriate to nucleophilic attacks.
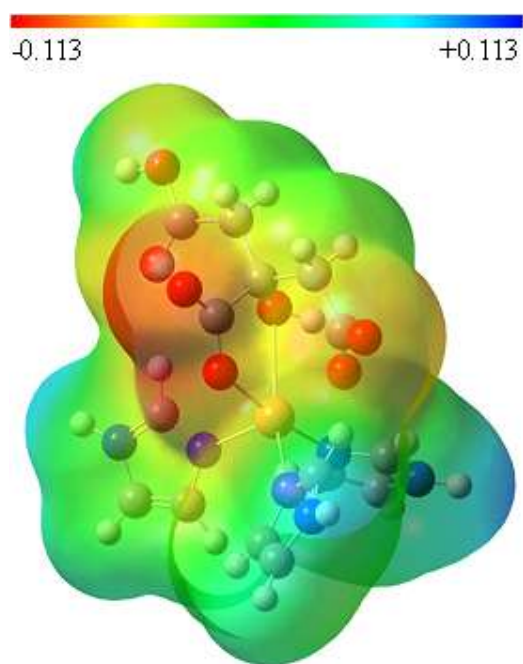
(a)
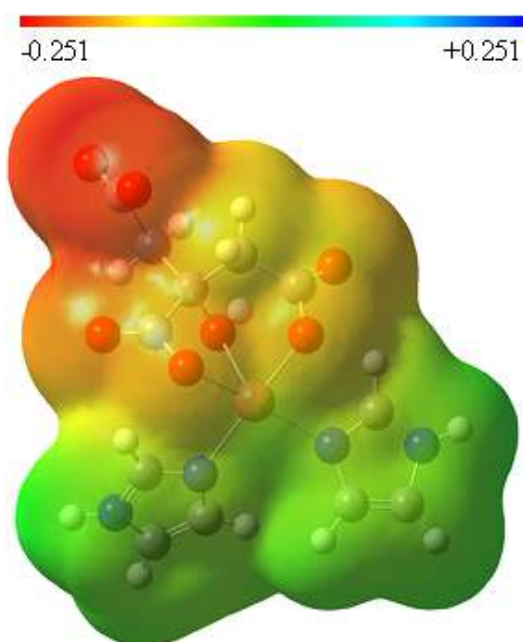
(b)

Figure 12. The molecular electrostatic potential maps of (a) (**1**) and (b) (**2**).

Electronic Structure Descriptors

The determination of the chemical reactivity ranking of the studied copper complexes could be achieved by calculating the electronic descriptors of their molecular structures. Thus, the energy of singly occupied molecular orbital (E_{SOMO}), the energy of the lowest unoccupied molecular orbital (E_{LUMO}), the energy gap (E_{GAP}), the chemical hardness (η), the chemical

softness (σ), the dipole moment (μ), the polarizability (α) and the hyperpolarizability (β) are calculated by using equations (1) – (5) and their values are given in Table 8.

Table 8.

Calculated electronic structure descriptors for the two studied complexes.

	E_{SOMO}[1]	E_{LUMO}[1]	I[1]	A[1]	E_{GAP}[1]
Complex (**1**)	-8.857	3.088	8.857	-3.088	11.945
Complex (**2**)	-4.611	4.311	4.611	-4.311	8.922
	η[1]	σ[2]	μ[3]	α[4]	β[4]
Complex (**1**)	5.972	0.167	12.955	189.785	106.681
Complex (**2**)	4.461	0.224	30.660	152.778	353.385

[1] in eV, [2] in eV^{-1}, [3] in Debye, [4] in a.u.

According to the values of Table 8, chemical reactivity increases with the increasing of E_{SOMO}, σ, μ, α and β. As a result, chemical reactivity ranking should be as follow:

Complex (**2**) > Complex (**1**) (in E_{SOMO}, σ, μ and β)

Complex (**1**) > Complex (**2**) (in α)

On the other hand, the chemical reactivity ranking increases with decreasing of E_{LUMO}, E_{GAP} and η. According to these parameters, the chemical reactivity ranking should be as follow:

Complex (**2**) > Complex (**1**) (in E_{GAP} and η)

Complex (**1**) > Complex (**2**) (in E_{LUMO})

And thus, complex (**2**) is more reactive than complex (**1**).

3.3.   Spectroscopic Study

The FT-IR spectra of the two complexes are illustrated in Figures S5a and S5b. The vibrational assignments have been made by comparison with the assignments reported earlier for similar imidazole and citrate systems. Similarly to other citrate-complexes [50], the

stretching frequency ν(O–H) of the citrate hydroxyl group occurs as a strong large band near 3157 cm^{-1} for complex (**1**) and is sharper for complex (**2**) appearing at 3150 cm^{-1}. Additionally, the ν(O–H) vibration of the protonated carboxyl moiety in (**1**) overlapped with the former frequency range. Furthermore, the antisymmetric ν_{as}(–CO$_2$) and the symmetric ν_s(–CO$_2$) carboxylate stretching vibrations for the coordinated citrate in (**1**) and (**2**) occur at (1647 and 1419 cm^{-1}) and at (1591 and 1381 cm^{-1}), respectively. The positions of these carboxylate stretching vibrations are within the range expected for carboxylate groups [51] and are shifted to lower frequencies compared to those of free citric acid [52], denoting changes in vibrational status upon complexation to copper. In the IR spectrum of (**1**), there is a strong sharp absorption band at 1735 cm^{-1} characteristic of the ν(CO$_2$H) stretching. This vibration is mainly resulting from the uncoordinated β-carboxylic acid group as it was observed in [53] at 1720 cm^{-1}, however, its absence from compound's (**2**) spectrum indicates the obvious deprotonation of the three carboxylic acid groups. In addition, sharp to medium bands at 523, 599 and 670 cm^{-1} are mainly generated by the (–CO$_2$) rocking, wagging and bending vibrations [54] in complex (**1**). The same vibration modes for (**2**) occur at about 537, 625 and 657 cm^{-1}. On the other hand, the two complexes exhibit infrared frequencies appearing as doublets and occurring at (3148, 3127 cm^{-1}) for (**1**) and at (3137, 3117 cm^{-1}) for (**2**), which are assigned to the ν(N–H) stretching bands of the coordinated imidazole ligands and the free imidazolium moieties. These frequencies are in the same values range of other related complexes based on imidazole [54], though show approximately (228 and 239 cm^{-1}) shifts to lower frequencies compared to the free imidazole molecule [55]. Therefore, the shifting size reflects the strength of the coordinated bond in the formed complexes between the imidazole nitrogens and the Cu(II) ions, as well as the their hydrogen bonds strength. It is worth noting that the medium broad bands appearing at around 3025-2971 and 3042-2937 cm^{-1}, in complex (**1**) and (**2**) respectively, are due the ν(C–H) absorption vibrations of the citrate together with the imidazole moieties, as reported in [52] and [56] at about 2994 and 3122-2973 cm^{-1}, respectively. It is to be noted that the experimental frequencies are supported by the calculated results.

Moreover, the broad bands at 1571 and 1587 cm^{-1} are assigned to the (N–H) in-plane bending vibrations in (**1**) and (**2**), respectively [56]. While a band at 1223 cm^{-1} has been observed in the case of the free imidazole molecule [55]. Due to the strong and moderate intermolecular

hydrogen bonds in (**1**) and (**2**) as seen in the crystal structure discussion, the frequencies of this vibration mode have shown an upward shift. Furthermore, both spectra show the presence of ν(C=C) and ν(C=N) stretching vibrations in the region 1535-1495 cm^{-1} and 1491-1447 cm^{-1}, respectively [57]. The two spectra respectively exhibit the following absorption frequencies: (1418, 1383, 1364, 941 cm^{-1}) and (1427, 1384, 1331, 959 cm^{-1}) attributed to the citrate (–CH$_2$) bending, wagging, twisting and rocking deformation modes [54]. Whereas, the (–CH) in-plane bending of the imidazole molecules occur in the 1260-1128 cm^{-1} range for (**1**) and 1263-1108 cm^{-1} for (**2**), and the out of-plane bending of the same bond appears for the two complexes at 1068 cm^{-1} as a very strong sharp band [54]. The bands at around 540/441 cm^{-1} for (**1**) and 584/432 cm^{-1} for (**2**) can be assigned to the ν(Cu–O) and ν(Cu–N) stretching vibrations [58].

3.4. Magnetic Properties

The magnetic susceptibility of the polycrystalline samples of (**1**) and (**2**) were examined in a magnetic field of 1000 Oe under the temperature range 2–300 K. The magnetic susceptibilities (χ_M) and their inverses ($1/\chi_M$) were plotted versus temperature, and the results are shown in Figures 13a and 13b. The magnetic susceptibility (χ_M) of both complexes (**1**) and (**2**) displays a paramagnetic behavior over most of the temperature range investigated. As can be seen in Figures 13a and 13b, it exhibits a Curie-Weiss dependence, and the whole susceptibility data was fitted to the expression $\chi_M = C_M/(T - \theta)$ affording molecular Curie constants C_M of 0.3936(9) and 0.3903(9) cm^3·K·mol^{-1} and Weiss constants θ of –0.2(2) and –0.9(1) K, respectively. The former values correspond to g-values of 2.414(4) for (**1**) and 2.252(2) for (**2**). Furthermore, the C value is in the expected range for an isolated Cu(II) ion and the small value of the Weiss constants, less than 1 K, suggests the existence of a very weak antiferromagnetic coupling (with the exchange coupling constant J found to be 0.3943(8) and 0.4174(5) cm^{-1} for complexes (**1**) and (**2**) respectively). Such behavior arises from the non-covalent interactions and the intermolecular hydrogen bonding transmitted through the Cu−O−C−C−C−O···H−O−Cu pathways [59] giving rise to binuclear hydrogen-bonded copper complexes (O7−H7···O3 hydrogen bonds) with Cu···Cu distances of 7.651 and 8.395 ♦, within complex (**1**) and (**2**) respectively (Figure S6).
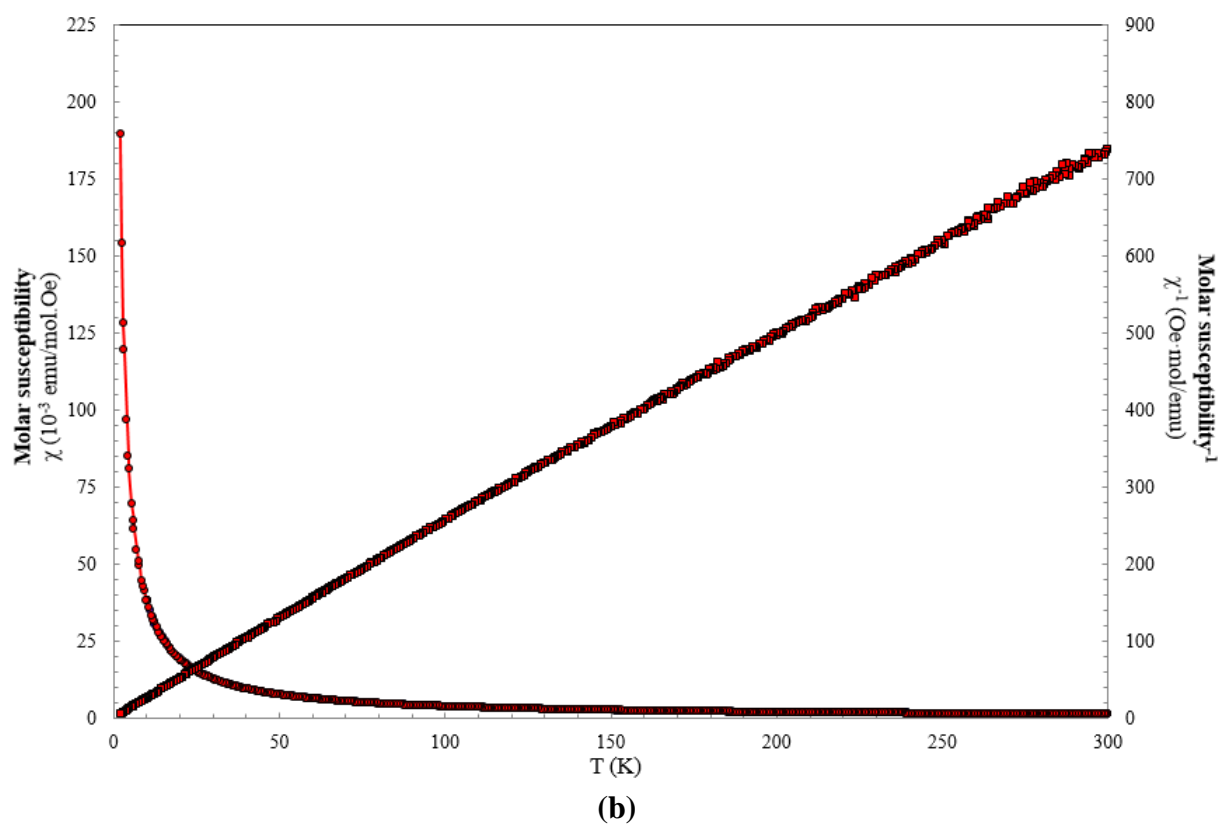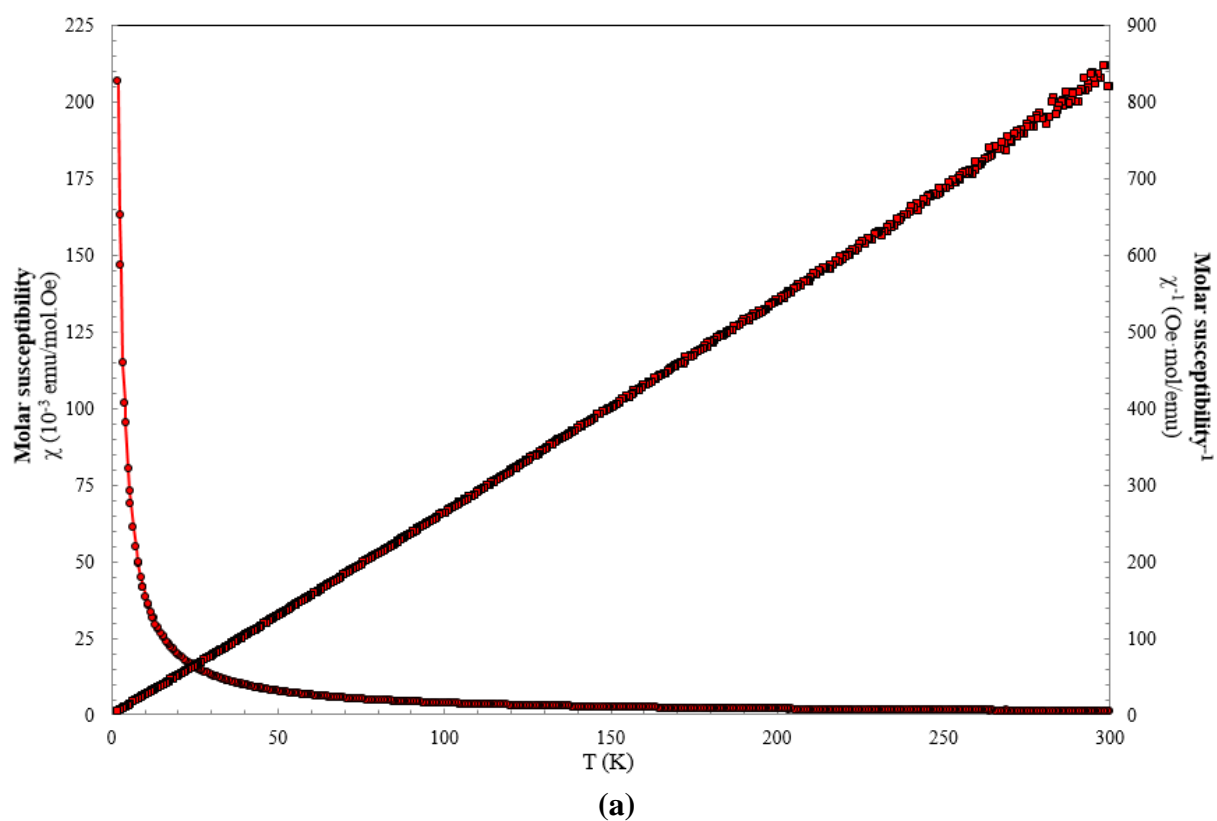
Figure 14. Temperature dependence of χ_M and $1/\chi_M$ measured under applied field of 1 kOe for (a) complex (**1**) and (b) complex (**2**).

Moreover, the weakly interacting monomeric Cu^{2+} ions might be resulting from the contribution of the following pathways effect; Cu−N−C−N−H⋯O−Cu infinite chains (N2B−H2NB⋯O5 and N2B−H2NB⋯O6 hydrogen bonds) in complex (**1**) and Cu−N−C−N−H⋯O−C−O−Cu binuclear units (N2A−H2NA⋯O2 hydrogen bonds) [32] observed in complex (**2**) which yield to the Cu⋯Cu separations of 7.209 and 7.403 ♦, respectively (Figure S6).

Moreover, $\chi_M T$ versus temperature plots show hardly any changes at lower temperatures and remain almost constant at values of 0.365–0.415 $cm^3 \cdot K \cdot mol^{-1}$ for complex (**1**) and 0.406–0.381 $cm^3 \cdot K \cdot mol^{-1}$ for complex (**2**) down to 2 K. Therefore, the effective magnetic moments μ_{eff} for (**1**) and (**2**), of 1.789 and 1.732 μ_B/Cu^{2+} respectively, are in the range expected for mononuclear pentacoordinated-copper(II) complexes [32,60], which corresponds to the spin-only value for one unpaired electron (namely 1.73 μ_B, for S = ½ and a spin-only g-value of 2.0) [61].

3.5. Biological Activity

After plates' incubation, zones of inhibition formed for each complex evaluated for its in vitro antibacterial activity against *Staphylococcus aureus* and *Escherichia coli* as examples of Gram-positive bacteria and Gram-negative bacteria, respectively, have been measured and accumulated in Table 9. Furthermore, the same table exhibits the results of the complexes' tests against two fungi; namely *Candida specie* and *Aspergillus niger*. Concentrations used were 10 $mg \cdot mL^{-1}$ (Concentration 1) and 20 $mg \cdot mL^{-1}$ (Concentration 2).

On the basis of the minimum inhibitory concentration (M.I.C) and the diameter of the inhibition zone, complex (**1**) shows highest fungicidal activity against *Aspergillus niger* (15 mm at 10 $mg \cdot mL^{-1}$) compared to its inhibition of *Candida specie* (10 mm at 10 $mg \cdot mL^{-1}$). The same behaviors have been observed for complex (**2**) for the two microorganisms but with higher response (20 mm at 10 $mg \cdot mL^{-1}$ for *Aspergillus niger vs.* 16 mm at 10 $mg \cdot mL^{-1}$ for *Candida specie*). Moreover, both complexes are found to have high activity against *Staphylococcus aureus* (15 mm for complex (**1**) and 18 mm for complex (**2**), at 10 $mg \cdot mL^{-1}$). Whereas, antibacterial activity of complex (**1**) against *Escherichia coli* is observed to be significant (10 mm at 20 $mg \cdot mL^{-1}$) compared to complex (**2**), which showed no effect on the same bacteria. Furthermore, complex (**2**) has the advantage of combining the free ligand and the coordinated-ligand molecule in its structure, and thus makes it more potent antifungal and

antibacterial agent compared to complex (**1**). This is in agreement with the literature [62,63] assuming that the coordination of an organic ligand to a metallic center magnifies its antimicrobial activity due to the greater lipophilic nature of the complex than the free ligand's one. Therefore, the overlapping of the ligand and the metallic cation orbitals amplifies the resonance of π electrons and consequently increases the liposolubility of the complex with respect to its free ligand [64]. This improved lipophilicity enhances the penetration of the complexes into lipid membrane and stops the metal binding sites on enzymes of microorganisms.

Table 9.

Diameter of the inhibition zone (mm) for the two complexes.

	Complex (**1**)		Complex (**2**)	
	$C_1 = 10$ mg·mL^{-1}	$C_2 = 20$ mg·mL^{-1}	$C_1 = 10$ mg·mL^{-1}	$C_2 = 20$ mg·mL^{-1}
Staphylococcus aureus	15	18	18	21
Escherichia coli	NE	10	NE	NE
Candida specie	10	13	16	21
Aspergillus niger	15	18	20	23

NE = No effect.

4. Conclusion :

Two new copper (II) complexes based on pyrazole and citrate ligands were prepared, characterized by single-crystal X-ray diffraction and FTIR spectroscopy, and their magnetic and biological properties were studied. The crystallographic study revealed that the complexes are pentacoordinated and form extensive 3D propagating frameworks as a result of strong and moderate O−H⋯O and N−H⋯O hydrogen-bonding patterns. The *Hirshfeld* surface analysis indicated that the two crystal structures are dominated by the O⋯H/H⋯O, H⋯H and C⋯H/H⋯C non-covalent interactions. Moreover, the N⋯H/H⋯N contacts exhibited a high propensity to form C−H⋯N interactions. While, the C⋯O and O⋯O contacts are very impoverished, and the $\pi\cdots lp$ interactions in (**2**) are over-represented with E_{CN} being 2.89. The FTIR vibrational absorptions are in full agreement with the

crystallographic data. In addition, computational investigations of the studied complexes were performed by using HF method with 6-31G(d)(LANL2DZ) mix basis sets in the gas phase. The geometric and spectral analyses showed an agreement with the experimental ones. Additionally, their MEP maps were examined and their chemical reactivity investigated by electronic structure descriptors, showing that complex (**2**) is more reactive than complex (**1**). The results of the temperature variable magnetic studies displayed a paramagnetic behavior of both compounds with a very weak antiferromagnetic coupling due to the Cu···Cu separations of about 7.5 ♦. The antimicrobial tests suggested that the two complexes are promising against *Staphylococcus aureus*, though complex (**1**) was found to be effective against *Escherichia coli*. Furthermore, (**1**) and (**2**) showed significant fungicidal activity against *Aspergillus niger* and *Candida specie*.

Appendix A. Supplementary material

Crystallographic data for the structural analysis of both new complexes have been deposited at the Cambridge Crystallographic Data Centre, CCDC No 1565437 and 1565432 for compounds (**1**) and (**2**) respectively. These data can be obtained free of charge via http://www.ccdc.cam.ac.uk/conts/retrieving.html, or from the CCDC, 12 Union Road, Cambridge, CB2 1EZ, UK: fax: (+44) 01223-336-033; e-mail: deposit@ccdc.cam.ac.

References

[1] A. Bhatnagar, P. K. Sharma & N. Kumar, *International J. Pharm. Tech. Research*, 2011, **3**(1), 268-282.

[2] (a) T. Nakamura, H. Kakinuma, H. Umemiya, H. Amada, N. Miyata, K. Taniguchi, K. Bando & M. Sato, *Bioorg. Med. Chem. Lett*, 2004, **14**, 333–336. (b) P. G. Nantermet, J. C. Barrow, S. R. Lindsley, M. Young, S. Mao, S. Carroll, C. Bailey, M. Bosserman, D. Colussi, D. R. McMasters, J. P. Vacca & H. G. Selnick, *Bioorg. Med. Chem. Lett*, 2004, **14**, 2141–2145. (c) S. Emami, A. Foroumadi, M. Falahati, E. Lotfali, S. Rajabalian, S. Ahmed Ebrahimi, S. Farahyarc & A. Shafiee, *Bioorg. Med. Chem. Lett*, 2008, **18**, 141–146.

[3] M. Maru & M. K. Shah, *J. Chem. Pharm. Research*, 2012, **4**(3), 1638-1643.

[4] J. Reedijk & E. Bouwman, *Bioinorganic Catalysis*, Marcel Dekker Inc., New York & Basel, 1999.

[5] K. D. Karlin & Z. Tyeklar, *Bioinorganic Chemistry of Copper*, Chapman & Hall, New York, 1993.

[6] E. Colacio, M. Ghazi, R. Kivekäs, M. Klinga, F. Lloret & J. M. Moreno, *Inorg. Chem*, 2000, **39**(13), 2770–2776.

[7] M. T. Caudle, J. W. Kampf, M. L. Kirk, P. G. Rasmussen & V. L. Pecoraro, *J. Am. Chem. Soc*, 1997, **119**(39), 9297–9298.

[8] (a) L. Casella, L. De Gioia, G. F. Silvestri, E. Monzani, C. Redaelli, R. Roncone & L. Santagostini, *J. Inorg. Biochem*, 2000, **79**, 31. (b) T. D. P. Stack, V. Mahadevan, M. J. Henson, J. L. Du Bois, B. Hedman, K. O. Hodgson & E. I. Solomon, *J. Inorg. Biochem*, 2001, **86**, 442. (c) Y. F. Song, C. Massera, P. Gamez, A. M. M. Lanfredi & J. Reedijk, *Eur. J. Inorg. Chem*, 2004, 3025.

[9] (a) S. M. Morehouse, A. Polychronopoulou & G. J. B. Williams, *Inorg. Chem*, 1980,**19**(12), 3558–3561. (b) G. Fransson & B. K. S. Lundberg, *Acta Chem. Scand.* A, 1974, **28**(5), 578–588. (c) D. L. McFadden, A. T. McPhail, C. D. Garner & F. E. Mabbs, J. *Chem. Soc., Dalton Trans,* 1976, 47–52.

[10] H. Beinert, *Coord. Chem. Rev*, 1980, **33**, 55.

[11] J. R. J. Sorrenson, *Prog. Med. Chem*, 1989, **26**, 437. (and references therein).

[12] A. L. Abuhijleh & C. Woods, *Inorg. Chim. Acta*, 1993, **209**, 187.

[13] H. Tamura, H. Imai, J. Kuwahara & Y. Sugiura, *J. Am. Chem. Soc*, 1987, **109**, 6870.

[14] C. P. Raptopoulu, S. Paschalidou, A. A. Pantazaki, A. Terzis, S. P. Perlepes, T. Lialiaris, E. G. Bakalbassis, J. Mrozinski & D. A. Kyriakidis, *J. Inorg. Biochem*, 1998, **71**, 15.

[15] (a) J. Server-Carrió, E. Eseriva & J-V. Folgado, *Trans. Met. Chem*, 1996, **21**, 541–545. (b) E. Suresh, *J. Chem. Cryst*, 2009, **39**, 104. (c) A. S. Antsyshkina, G. G. Sadikov, A. L.

Poznyak & V. S. Sergienko, *Russ. J. Inorg. Chem*, 2006, **51**, 283. (d) X. You, L. Zhu & J. Sun, *Chin. J. Chem*, 2010, **28**, 2174. (e) C. K. Prout, G. B. Allison & F. J. C. Rossotti, *J. Chem. Soc. A*, 1971, 3331–3335. (f) R. Koner & I. Goldberg, *Acta Cryst*, 2009, C**65**, m37. (g) J. K. Nath, A. M. Kirillov & J. B. Baruah, *RSC Advances*, 2014, **4**, 47876. (h) L.-Q. Xiao, J.-Z. Qiao & T.-P. Hu, *Chin. J. Inorg. Chem*, 2014, **30**, 2127. (i) A. L. Abuhijleh & C. Woods, *Inorg. Chim. Acta*, 1992, **194**, 9. (j) D.-D. Lin & D.-J. Xu, *J. Coord. Chem*, 2005, **58**, 605.

[16] (a) S. Wang, M.-L. Hu, J.-X. Yuan, Y.-Q. Cheng, J.-J. Lin & Z.-Y. Huang, *Chin. J. Chem*, 2000, **18**, 546. (b) A. Benkanoun, F. Balegroune, A. Guehria-Laidoudi, S. Dahaoui & C. Lecomte, *Acta Cryst*, 2012, E**68**, m480. (c) Y. Wu, L. Yu, M. Cheng, W. Han, L. Wang, X. Guo & Q. Liu, *Chin. J. Chem*, 2012, **30**, 1045. (d) E. Suresh, M. M. Bhadbhade & K. Venkatasubramanian, *Polyhedron*, 1999, **18**, 657. (e) Z. M. Jin, L. He, L. Shen, M. C. Li & M. L. Hu, *Acta Cryst*, 2003, E**59**, m1053. (f) K.-L. Zhang, H.-W. Kuai, W.-L. Liu & G.-W. Diao, *J. Mol. Struct*, 2007, **831**, 114.

[17] (a) D.-D. Lin & D.-J. Xu, *Acta Cryst*, 2005, E**61**, m1215. (b) Y.-Q. Cheng, W.-J. Lin, M.-L. Hu, J.-X. Yuan, S. Wang & J.-G. Wang, *Chin. J. Chem*, 2001, **19**, 321. (c) I. G. Filippova, O. A. Gerco, Y.A. Simonov, A. A. Deseatnic-Ciloci, S. F. Clapco, J. P. Tiurin & S. G. Baca, *Polyhedron*, 2010, **29**, 1102. (d) F. Guo, X. Zhang, B. Zhu & J. Qiu, *J. Inorg. Organomet. Polym. Mater*, 2010, **20**, 38. (e) D. Cheng, M. A. Khan & R. P. Houser, *Inorg. Chim. Acta*, 2003, **351**, 242. (f) P. Naumov, M. Ristova, M. G. B. Drew & S. W. Ng, *Acta Cryst*, 2000, C**56**, e372. (g) Q. Zhang & C. Lu, *J. Chem. Cryst*, 2005, **35**, 965. (h) K.-L., Zhang, G.-W. Diao & S. W. Ng, *Acta Cryst*, 2010, E**66**, m1430. (i) Y.-J. Wang, Y.-Y. Wang, J. Feng & Q.-Y. Lin, *Z. Kristallogr*, 2009, **224**, 549. (j) L.-P. Sun, S.-Y. Niu, J. Jin, G.-D. Yang & L. Ye, *Inorg. Chem. Commun*, 2006, **9**, 679.

[18] (a) N. Zhao, Z. Lian, T., Lou, J. Zhang, X. Li & P. Liu, *Z. Kristallogr*, 2009, **224**, 463. (b) M. Hu, D. Cheng, J. Liu & D. Xu, *J. Coord. Chem*, 2001, **53**, 7. (c) Y.-D. Wang, X.-H. Wu, Q.-X. Zeng & Y.-W. Yao, *Chin. J. Struct. Chem*, 2005, **24**,641. (d) J.-R. Su, K.-L. Yin & D.-J. Xu, *Chin. J. Struct. Chem*, 2004, **23**, 399. (e) H.-J. Chen & Y.-G. Li, *J. Coord. Chem.*, 2008, **61**, 2150.

[19] (a) L. Yue, Q.-X. Zhou, Y.-J. Wang & X.-Q. Zhao, *Chin. J. Struct. Chem*, 2005, **24**, 287. (b) C. An, X. Feng, N. Zhao, P. Liu, T. Wang & Z. Lian, *J. Cluster Sci*, 2015, **26**, 889. (c) S. Gao, J.-W. Liu, L.-H. Huo, H. Zhao & J.-G. Zhao, *Acta Cryst*, 2004, E**60**, m1308. (d) G.

Gunay, O. Z. Yesilel, C. Darcan, S. Keskin & O. Buyukgungor, *Inorg. Chim. Acta*, 2013, **399**, 19.

[20] C. Sudha, S. K. Mandal & A. R. Chakravarty, *Inorg. Chem*, 1998, **37**, 270.

[21] Y.-F. Deng, Z.-H. Zhou, Z.-X. Cao & K.-R. Tsai, *J. Inorg. Biochem*, 2004, **98**, 1110.

[22] *APEX2*, *SADABS* and *SAINT*. Bruker AXS Inc., Madison, Wisconsin, USA. 2008.

[23] L. J. Farrugia, *J. Appl. Cryst*, 2012, **45**, 849–854.

[24] M. C. Burla, R. Caliandro, B. Carrozzini, G. L. Cascarano, C. Cuocci, C. Giacovazzo, M. Mallamo, A. Mazzone & G. Polidori, *J. Appl. Cryst,* 2015, **48**, 306-309.

[25] G. M. Sheldrick, *Acta Cryst*, 2015, C**71**, 3-8.

[26] C. F. Macrae, I. J. Bruno, J. A. Chisholm, P. R. Edgington, P. McCabe, E. Pidcock, L. Rodriguez-Monge, R. Taylor, J. van de Streek & P. A. Wood, *J. Appl. Cryst,* 2008, **41**, 466–470.

[27] S. P. Westrip, *J. Appl. Cryst,* 2010, **43**, 920–925.

[28] R. Dennington, T. Keith & J. Millam, *GaussView*, Version 5, Semichem Inc., Shawnee Mission, KS, 2009.

[29] M. J. Frisch, G. W. Trucks, H. B. Schlegel, G. E. Scuseria, M. A. Robb, J. R. Cheeseman, G. Scalmani, V. Barone, B. Mennucci, G. A. Petersson, H. Nakatsuji, M. Caricato, X. Li, H. P. Hratchian, A. F. Izmaylov, J. Bloino, G. Zheng, J. L. Sonnenberg, M. Hada, M. Ehara, K. Toyota, R. Fukuda, J. Hasegawa, M. Ishida, T. Nakajima, Y. Honda, O. Kitao, H. Nakai, T. Vreven, J. A. Montgomery, Jr., J. E. Peralta, F. Ogliaro, M. Bearpark, J. J. Heyd, E. Brothers, K. N. Kudin, V. N. Staroverov, R. Kobayashi, J. Normand, K. Raghavachari, A. Rendell, J. C. Burant, S. S. Iyengar, J. Tomasi, M. Cossi, N. Rega, J. M. Millam, M. Klene, J. E. Knox, J. B. Cross, V. Bakken, C. Adamo, J. Jaramillo, R. Gomperts, R. E. Stratmann, O. Yazyev, A. J. Austin, R. Cammi, C. Pomelli, J. W. Ochterski, R. L. Martin, K. Morokuma, V. G. Zakrzewski, G. A. Voth, P. Salvador, J. J. Dannenberg, S. Dapprich, A. D. Daniels, Ö. Farkas, J. B. Foresman, J. V. Ortiz, J. Cioslowski & D. J. Fox, *Gaussian 09*, Revision A.02, Gaussian, Inc., Wallingford CT, 2009.

[30] A.W. Addison, T.N. Rao, J. Reedijk, J. van Rijn & G.C. Verschoor, *J. Chem. Soc., Dalton Trans*, 1984, 1349.

[31] J. Sanchiz, Y. Rodríguez-Martín, C. Ruiz-Pérez, A. Mederos, F. Lloret & M. Julve, *New J. Chem*, 2002, **26**, 1624-1628.

[32] R. Carballo, A. Castiñeiras, B. Covelo, E. García-Martínez, J. Niclós & E.M. Vázquez-López, *Polyhedron*, 2004, **23**, 1505–1518.

[33] A. T. Çolak, F. Çolak, D. Akduman, O. Z. Yeşilel & O. Büyükgüngör, *Solid State Sciences*, 2009, **11**, 1908–1918.

[34] (a) A. L. Abuhijleh, C. Woods, *Inorg. Chem. Commun*, 2001, **4**, 119-123. (b) A. Vlad, M.-F. Zaltariov, S. Shova, G. Novitchi, C.-D. Varganici, C. Train & M. Cazacu, *CrystEngComm*, 2013, **1** (5), 5368–5375. (c) W. Wolodkiewicz, *J. Coord. Chem*, 2002, **55**,727.

[35] G. Zhang, G. Yang & J. S. Ma, *Cryst.Growth Des*, 2006, **6**, 375.

[36] R. Moreno-Fuquen, J. Ellena & J. E. Theodoro, *Acta Cryst*, 2009, E**65**, o2717.

[37] V. H. Rodrigues, M. M. R. R. Costa, E. de Matos Gomes & M. S. Belsley, *Acta Cryst*, 2007, E**63**, o4031.

[38] D.-J. Yang, *Acta Cryst*, 2007, E**63**, o4038.

[39] D.-D. Lin, J.-G. Liu & D.-J. Xu, *Acta Cryst*, 2006, E**62**, o451–o452.

[40] Z.-X. Liu, *Acta Cryst*, 2009, E**65**, o499.

[41] J. Bernstein, R. E. Davis, L. Shimoni & N.-L. Chang, *Angew. Chem. Int. Ed. Engl*, 1995, **34**, 1555–1573.

[42] M. A. Spackman & D. Jayatilaka, *CrystEngComm*, 2009, **11**, 19–32.

[43] M. Spackman & J. J. McKinnon, *Cryst Eng Comm*, 2002, **4**, 378.

[44] S. K. Wolff, D. J. Grimwood, J. J. McKinnon, M. J. Turner, D. Jayatilaka & M. A. Spackman, *Crystal Explorer*, 2012, University of Western Australia, Perth.

[45] B. Guillot, E. Enrique, L. Huder & C. Jelsch, *Acta Cryst*, 2014, A**70**, C279.

[46] C. Jelsch, K. Ejsmont & L. Huder, *IUCrJ*, 2014, **1**, 119.

[47] (a) W. E. Klee, *Cryst. Res. Technol*, 2004, **39**, 959–968. (b) J.-G. Eon, *Acta Cryst*, 2005, A**61**, 501–511. (c) O. Delgado-Friedrichs & M. O'Keeffe, *J. Solid State Chem*, 2005, **178**, 2480–2485.

[48] (a) A. F. Wells, *Three-Dimensional Nets and Polyhedra*, 1977, New York: Interscience. (b) L. Öhrström & K. Larsson, *Molecule-Based Materials: The Structural Network Approach*, 2005, Amsterdam: Elsevier. (c) L. Carlucci, G. Ciani & D. M. Proserpio, *Making Crystals by Design. Methods, Techniques and Applications*, 2007, Edited by D. Braga & F. Grepioni, Wiley : Darmstadt.

[49] V. A. Blatov, A. P. Shevchenko & D. M. Proserpio, *Cryst. Growth Des*, 2014, **14**, 3576-3586.

[50] P. Che, D. Fang, D. Zhang, J. Feng, J. Wang, N. Hu & J. Meng, *Journal of Coordination Chemistry*, 2005, **58** (17), 1581–1588.

[51] Y.-F. Deng & Z.-H. Zhou, *Journal of Coordination Chemistry*, 2009, **62** (5), 778–788.

[52] (a) L. Bellamy, *The Infrared Spectra of Complex Molecules*, 1958, Wiley: New York. (b) L. C. Bichara, H. E. Lanús, E. G. Ferrer, M. B. Gramajo & S. A. Brandán, *Advan. Phys. Chem*, 2011, **347072**, 1-10. (c) R.-H. Zhang, X.-W. Zhou, Y.-C. Guo, M.-L. Chen, Z.-X. Cao, Y. L. Chow & Z.-H. Zhou. *Inorganica Chimica Acta*, 2013, **406**, 27–36.

[53] A. Selvam, S. Pandi, S. Selvakumar & S. Srinivasan, *Archives of Applied Science Research*, 2012, **4** (6), 2474-2478.

[54] H.-J. Chen, J. Zhang, W.-L. Feng & M. Fu, *Inorganic Chemistry Communications*, 2006, **9**, 300–303.

[55] R. Ramasamy, *Armenian Journal of Physics*, 2015, **8**(1), 51-55

[56] B. Morzyk-Ociepa, E. Rózycka-Sokołowska & D. Michalska, *Journal of Molecular Structure*, 2012, **1028**, 49–56.

[57] V. Krishnakumar & R. Ramasamy, *Indian J. Pure & Appl. Phys*, 2002, **40**, 252.

[58] A. S. Mahdi, A. A. Awad & M. M. Hasson, *Acta Chim Pharm Indica*, 2017, **7** (1), 1-7.

[59] T. Ohmura, W. Mori, T. Takei, T. Ikeda & A. Maeda, *Materials Science-Poland*, 2005, **23**(3), 729-736.

[60] (a) B. Żurowska & J. Mroziński, *Materials Science-Poland*, 2005, **23**(3), 737-744. (b) S. K. Jain, B. S. Garg, Y. K. Bhoon, D. L. Klayman & J. P. Scovill, 1985, *Spectrochim. Acta*, **41**A, 407. (c) A. Bottcher, H. Elias, E. Jager, H. Lanffelderova, M. Mazur, L. Mullor, H. Paulas, P. Pelikan, M. Rudolph & M. Valko, *Inorg. Chem*, 1993, **32**, 4131.

[61] J. M. D. Coey, *Magnetism and Magnetic Materials*, 2010, Cambridge University Press.

[62] Y. Anjaneyulu & R. P. Rao, *Synth. React. Inorg. Met. Org. Chem*, 1986, **16**, 257.

[63] M. Montazerozohori, S. Zahedi, M. N. Esfahani & A. Naghiha, *J. Ind. Eng. Chem*, 2014, **20**, 2463.

[64] N. Dharmaraj, P. Viswanathamurthi & K. Natarajan, *Transit. Met. Chem*, 2001, **26**, 105.